Electronic Supplementary Material (ESI) for Chemical Science.
This journal is © The Royal Society of Chemistry 2023

Supporting Information

for

Isostructural Bridging Diferrous Chalcogenide Cores $[Fe^{II}(\mu\text{-}E)Fe^{II}]$ (E = O, S, Se, Te) with Decreasing Antiferromagnetic Coupling Down the Chalcogenide Series.

Ethan Zars,[a] Lisa Gravogl,[b] Michael R. Gau,[a] Patrick J. Carroll,[a] Karsten Meyer,[b,*] and Daniel J. Mindiola[a,*]

[a]*Department of Chemistry, University of Pennsylvania, Philadelphia, Pennsylvania 19104, United States*

[b]*Department of Chemistry & Pharmacy, Friedrich-Alexander-Universität Erlangen – Nürnberg. Erlangen, Bavaria, 91058, Germany*

[*]*Corresponding Authors: Daniel J. Mindiola, email: mindiola@sas.upenn.edu, Karsten Meyer, email: karsten.meyer@fau.de*

1 Contents

1 Contents **(S2)**

2 Materials and Methods **(S4)**

3 Syntheses

3.1 Synthesis of ($^{t\mathrm{Bu}}$pyrpyrr$_2$)Fe(OPPh$_3$) (**1-O$^{\mathbf{Ph}}$**) **(S7)**

3.2 Synthesis of ($^{t\mathrm{Bu}}$pyrpyrr$_2$)Fe(SPPh$_3$) (**1-S$^{\mathbf{Ph}}$**) **(S7)**

3.3 Synthesis of ($^{t\mathrm{Bu}}$pyrpyrr$_2$)Fe(SePPh$_3$) (**1-Se$^{\mathbf{Ph}}$**) **(S8)**

3.4 Synthesis of ($^{t\mathrm{Bu}}$pyrpyrr$_2$)Fe(TeP^{t}Bu$_3$) (**1-Te$^{\boldsymbol{t\mathrm{Bu}}}$**) **(S9)**

3.5 Synthesis of [K]$_2$[($^{t\mathrm{Bu}}$pyrpyrr$_2$)Fe$_2$(μ-O)] (**2-O**) **(S10)**

3.6 Synthesis of [K]$_2$[($^{t\mathrm{Bu}}$pyrpyrr$_2$)Fe$_2$(μ-S)] (**2-S**) **(S11)**

3.7 Synthesis of [K]$_2$[($^{t\mathrm{Bu}}$pyrpyrr$_2$)Fe$_2$(μ-Se)] (**2-Se**) **(S11)**

3.8 Synthesis of [K]$_2$[($^{t\mathrm{Bu}}$pyrpyrr$_2$)Fe$_2$(μ-Te)] (**2-Te**) **(S12)**

4 ^{1}H NMR Spectroscopy

4.1 ^{1}H NMR Spectrum of ($^{t\mathrm{Bu}}$pyrpyrr$_2$)Fe(OPPh$_3$) (**1-O$^{\mathbf{Ph}}$**) **(S14)**

4.2 ^{1}H NMR Spectrum of ($^{t\mathrm{Bu}}$pyrpyrr$_2$)Fe(SPPh$_3$) (**1-S$^{\mathbf{Ph}}$**) **(S15)**

4.3 ^{1}H NMR Spectrum of ($^{t\mathrm{Bu}}$pyrpyrr$_2$)Fe(SePPh$_3$) (**1-Se$^{\mathbf{Ph}}$**) **(S16)**

4.4 ^{1}H NMR Spectrum of ($^{t\mathrm{Bu}}$pyrpyrr$_2$)Fe(TeP^{t}Bu$_3$) (**1-Te$^{\boldsymbol{t\mathrm{Bu}}}$**) **(S17)**

4.5 ^{1}H NMR Spectrum of [K]$_2$[($^{t\mathrm{Bu}}$pyrpyrr$_2$)Fe$_2$(μ-O)] (**2-O**) **(S18)**

4.6 ^{1}H NMR Spectrum of [K]$_2$[($^{t\mathrm{Bu}}$pyrpyrr$_2$)Fe$_2$(μ-S)] (**2-S**) **(S19)**

4.7 ^{1}H NMR Spectrum of [K]$_2$[($^{t\mathrm{Bu}}$pyrpyrr$_2$)Fe$_2$(μ-Se)] (**2-Se**) **(S20)**

4.8 ^{1}H NMR Spectrum of [K]$_2$[($^{t\mathrm{Bu}}$pyrpyrr$_2$)Fe$_2$(μ-Te)] (**2-Te**) **(S21)**

5 UV-Vis Spectroscopy

5.1 UV-Vis Spectrum of ($^{t\mathrm{Bu}}$pyrpyrr$_2$)Fe(OPPh$_3$) (**1-O$^{\mathbf{Ph}}$**) **(S22)**

5.2 UV-Vis Spectrum of ($^{t\mathrm{Bu}}$pyrpyrr$_2$)Fe(SPPh$_3$) (**1-S$^{\mathbf{Ph}}$**) **(S23)**

5.3 UV-Vis Spectrum of ($^{t\mathrm{Bu}}$pyrpyrr$_2$)Fe(SePPh$_3$) (**1-Se$^{\mathbf{Ph}}$**) **(S24)**

5.4 UV-Vis Spectrum of ($^{t\mathrm{Bu}}$pyrpyrr$_2$)Fe(TeP^{t}Bu$_3$) (**1-Te$^{\boldsymbol{t\mathrm{Bu}}}$**) **(S25)**

5.5 UV-Vis Spectrum of [K]$_2$[($^{t\mathrm{Bu}}$pyrpyrr$_2$)Fe$_2$(μ-O)] (**2-O**) **(S26)**

5.6 UV-Vis Spectrum of [K]$_2$[($^{t\mathrm{Bu}}$pyrpyrr$_2$)Fe$_2$(μ-S)] (**2-S**) **(S27)**

5.7 UV-Vis Spectrum of [K]$_2$[($^{t\mathrm{Bu}}$pyrpyrr$_2$)Fe$_2$(μ-Se)] (**2-Se**) **(S28)**

5.8 UV-Vis Spectrum of [K]$_2$[($^{t\mathrm{Bu}}$pyrpyrr$_2$)Fe$_2$(μ-Te)] (**2-Te**) **(S29)**

6 Mössbauer Spectroscopy

6.1 Mössbauer Spectrum of ($^{t\mathrm{Bu}}$pyrpyrr$_2$)Fe(OPPh$_3$) (**1-O$^{\mathbf{Ph}}$**) **(S30)**

6.2 Mössbauer Spectrum of ($^{t\text{Bu}}$pyrpyrr$_2$)Fe(SPPh$_3$) (**1-S$^{\text{Ph}}$**) **(S31)**
6.3 Mössbauer Spectrum of ($^{t\text{Bu}}$pyrpyrr$_2$)Fe(SePPh$_3$) (**1-Se$^{\text{Ph}}$**) **(S32)**
6.4 Mössbauer Spectrum of ($^{t\text{Bu}}$pyrpyrr$_2$)Fe(TeP^{t}Bu$_3$) (**1-Te$^{t\text{Bu}}$**) **(S33)**
6.5 Mössbauer Spectrum of [K]$_2$[($^{t\text{Bu}}$pyrpyrr$_2$)Fe$_2$(μ-O)] (**2-O**) **(S34)**
6.6 Mössbauer Spectrum of [K]$_2$[($^{t\text{Bu}}$pyrpyrr$_2$)Fe$_2$(μ-S)] (**2-S**) **(S35)**
6.7 Mössbauer Spectrum of [K]$_2$[($^{t\text{Bu}}$pyrpyrr$_2$)Fe$_2$(μ-Se)] (**2-Se**) **(S36)**
6.8 Mössbauer Spectrum of [K]$_2$[($^{t\text{Bu}}$pyrpyrr$_2$)Fe$_2$(μ-Te)] (**2-Te**) **(S37)**

7 SQUID Magnetometry

7.1 SQUID Plot of ($^{t\text{Bu}}$pyrpyrr$_2$)Fe(OPPh$_3$) (**1-O$^{\text{Ph}}$**) Sample 1 **(S38)**
7.2 SQUID Plot of ($^{t\text{Bu}}$pyrpyrr$_2$)Fe(OPPh$_3$) (**1-O$^{\text{Ph}}$**) Sample 2 **(S39)**
7.3 Combined SQUID Plot of ($^{t\text{Bu}}$pyrpyrr$_2$)Fe(OPPh$_3$) (**1-O$^{\text{Ph}}$**) Sample 1 and Sample 2 **(S40)**
7.4 SQUID Plot of ($^{t\text{Bu}}$pyrpyrr$_2$)Fe(SPPh$_3$) (**1-S$^{\text{Ph}}$**) Sample 1 **(S41)**
7.5 SQUID Plot of ($^{t\text{Bu}}$pyrpyrr$_2$)Fe(SPPh$_3$) (**1-S$^{\text{Ph}}$**) Sample 2 **(S42)**
7.6 Combined SQUID Plot of ($^{t\text{Bu}}$pyrpyrr$_2$)Fe(SPPh$_3$) (**1-S$^{\text{Ph}}$**) Sample 1 and Sample 2 **(S43)**
7.7 SQUID Plot of ($^{t\text{Bu}}$pyrpyrr$_2$)Fe(SePPh$_3$) (**1-Se$^{\text{Ph}}$**) Sample 1 **(S44)**
7.8 SQUID Plot of ($^{t\text{Bu}}$pyrpyrr$_2$)Fe(SePPh$_3$) (**1-Se$^{\text{Ph}}$**) Sample 2 **(S45)**
7.9 Combined SQUID Plot of ($^{t\text{Bu}}$pyrpyrr$_2$)Fe(SePPh$_3$) (**1-Se$^{\text{Ph}}$**) Sample 1 and Sample 2 **(S46)**
7.10 SQUID Plot of ($^{t\text{Bu}}$pyrpyrr$_2$)Fe(TeP^{t}Bu$_3$) (**1-Te$^{t\text{Bu}}$**) Sample 1 **(S47)**
7.11 SQUID Plot of ($^{t\text{Bu}}$pyrpyrr$_2$)Fe(TeP^{t}Bu$_3$) (**1-Te$^{t\text{Bu}}$**) Sample 2 **(S48)**
7.12 Combined SQUID Plot of ($^{t\text{Bu}}$pyrpyrr$_2$)Fe(TeP^{t}Bu$_3$) (**1-Te$^{t\text{Bu}}$**) Sample 1 and Sample 2 **(S49)**
7.13 SQUID Plot of [K]$_2$[($^{t\text{Bu}}$pyrpyrr$_2$)Fe$_2$(μ-O)] (**2-O**) Sample 1 **(S50)**
7.14 Combined SQUID Plot of [K]$_2$[($^{t\text{Bu}}$pyrpyrr$_2$)Fe$_2$(μ-O)] (**2-O**) Sample 1 and Sample 2 **(S51)**
7.15 SQUID Plot of [K]$_2$[($^{t\text{Bu}}$pyrpyrr$_2$)Fe$_2$(μ-S)] (**2-S**) Sample 1 **(S52)**
7.16 Combined SQUID Plot of [K]$_2$[($^{t\text{Bu}}$pyrpyrr$_2$)Fe$_2$(μ-S)] (**2-S**) Sample 1 and Sample 2 **(S53)**
7.17 VTVF SQUID Plot of [K]$_2$[($^{t\text{Bu}}$pyrpyrr$_2$)Fe$_2$(μ-S)] (**2-S**) Sample 1 **(S54)**
7.18 SQUID Plot of [K]$_2$[($^{t\text{Bu}}$pyrpyrr$_2$)Fe$_2$(μ-Se)] (**2-Se**) Sample 1 **(S55)**
7.19 Combined SQUID Plot of [K]$_2$[($^{t\text{Bu}}$pyrpyrr$_2$)Fe$_2$(μ-Se)] (**2-Se**) Sample 1 and Sample 2 **(S56)**
7.20 VTVF SQUID Plot of [K]$_2$[($^{t\text{Bu}}$pyrpyrr$_2$)Fe$_2$(μ-Se)] (**2-Se**) Sample 1 **(S57)**
7.21 SQUID Plot of [K]$_2$[($^{t\text{Bu}}$pyrpyrr$_2$)Fe$_2$(μ-Te)] (**2-Te**) Sample 1 **(S58)**
7.22 Combined SQUID Plot of [K]$_2$[($^{t\text{Bu}}$pyrpyrr$_2$)Fe$_2$(μ-Te)] (**2-Te**) Sample 1 and Sample 2 **(S59)**

8 Crystallographic Information **(S60)**

9 References **(S63)**

2 Materials and Methods

General Considerations. All air sensitive manipulations were carried out in a MBraun Labmaster glovebox or using standard high vacuum Schlenk techniques under an N_2 atmosphere unless otherwise stated. Solvents were purchased from Fisher Scientific, sparged with argon gas for 20 minutes and dried by passing through two columns of Q5 Alumina and transferred to the glovebox in thick-walled reaction vessels. All solvents were stored over 4Å molecular sieves and sodium chunks inside the glovebox. Molecular sieves, alumina, and celite were activated by heating to 250 °C under dynamic vacuum overnight. Deuterated benzene was purchased from Cambridge Isotope Laboratories, dried over a potassium mirror overnight, degassed, and vacuum transferred into a 100 mL Schlenk tube before being brought into the glovebox for use. 3,5-^{t}Bu$_2$-bis(pyrrolyl)pyridine ($^{t\text{Bu}}$pyrpyrr$_2$H$_2$),[1] [Fe{N(SiMe$_3$)$_2$}$_2$],[2] [K]$_2$[($^{t\text{Bu}}$pyrpyrr$_2$)Fe$_2$(μ-N$_2$)],[3] ($^{t\text{Bu}}$pyrpyrr$_2$)Fe(OEt$_2$),[4] mesityl nitrile oxide (MesCNO),[5] triphenyl phosphine sulfide (S=PPh$_3$),[6] triphenyl phosphine selenide (Se=PPh$_3$),[7] and tritertbutyl phosphine telluride (Te=P^{t}Bu$_3$)[8] were synthesized according to literature procedures. KC_8 was prepared by heating one equivalent of potassium metal with one equivalent of graphite at 150 °C for 1 hour in a sealed reaction vessel under a N_2 atmosphere until all metallic potassium was reacted (*caution: KC_8 is a strong alkali metal reductant and is highly pyrophoric. Extreme care must be taken when preparing and handling this reagent to avoid laboratory fires caused by exposure to air and water. Excess KC_8 can be safely quenched using a tetrahydrofuran solution of benzoic acid under an inert atmosphere*). Triphenyl phosphine oxide (O=PPh$_3$) was purchased from Fisher Scientific and used without further purification. Tritertbutyl phosphine (P^{t}Bu$_3$) was purchased from Sigma Aldrich and used without further purification. Scintillation vials were washed first with acid and acetone followed by overnight submersion in a base bath and acid bath, and finally rinsed with DI water

and acetone. All glassware was rigorously cleaned using acetone, dilute acid solution, and DI water immediately after use and stored in a 120 °C oven for at least one day before being brought into the glovebox under overnight vacuum. Elemental analysis was conducted by Midwest Microlabs (Indianapolis, IN, USA). All NMR spectra were collected on a Bruker AVII-500 MHz instrument. ^{1}H NMR chemical shifts were referenced to the corresponding solvent residual signal. UV-vis spectroscopic studies were carried out using a Cary 5000 Spectrometer equipped with 1 cm quartz cuvettes sealed with J. Young valves. Solution state magnetic moments were calculated using Evans' Method. Diamagnetic corrections were applied assuming solvation by one hexane molecule (*t*Bupyrpyrr$_2$)Fe(OPPh$_3$), one toluene molecule for ($^{t\text{Bu}}$pyrpyrr$_2$)Fe(SePPh$_3$), and three toluene molecules for each of the anionic complexes [K]$_2$[($^{t\text{Bu}}$pyrpyrr$_2$)Fe$_2$(μ-E)] consistent with their ^{1}H NMR spectra and purification methods.[9]

Zero-field ^{57}Fe-Mössbauer spectra were recorded on a WissEl Mössbauer spectrometer (MRG-500) at a temperature of 77 K in constant acceleration mode. ^{57}Co/Rh was used as γ-radiation source. WinNormos for Igor Pro software was used for the quantitative evaluation of the spectral parameters (least squares fitting to Lorentzian peaks). The minimum experimental line widths were 0.21 mm·s^{-1} (full width at half maximum, FWHM). The temperature of the sample was controlled by a MBBC-HE0106 MÖSSBAUER He/N$_2$ cryostat within an accuracy of +/–0.3 K. Least-square fitting of the Lorentzian signals was carried out with the "Mfit" software, developed by Dr. Eckhard Bill (MPI CEC, Mülheim/Ruhr).[10] The isomer shifts were reported relative to α-iron reference at 300 K.

Magnetism data of microcrystalline and powdered samples (4.8–33.9 mg), loaded within a polycarbonate gel capsule inside a plastic straw or loaded and compressed into a quartz glass holder, were collected on a Quantum Design MPMS-3 SQUID magnetometer. The DC moment

was recorded in the temperature range of 2–300 K with an applied DC field of 1 T, if not stated otherwise. The DC moment was converted into molar magnetic susceptibility (χ_M) using the following formula (with H = magnetic field, n = moles of substance):

$$\chi_M = \frac{DC\ moment}{H \cdot n}$$

Values of the magnetic susceptibility were corrected for core diamagnetism of the sample using tabulated Pascal's constants.[11] Effective magnetic moments (μ_{eff}) were calculated using the following formula (with temperature (T)):

$$\mu_{eff} = 2.828 \cdot \sqrt{(\chi_M - \chi_{dia}) \cdot T}$$

For simulation and analysis of the data, the program "JulX2", written by Dr. Eckhard Bill (MPI CEC, Mülheim/Ruhr) was used.[12]

3 Syntheses

3.1 Synthesis of (^{tBu}pyrpyrr$_2$)Fe(OPPh$_3$) (1-O^{Ph}). 112.2 mg (^{tBu}pyrpyrr$_2$)Fe(OEt$_2$) (0.2 mmol) was dissolved in 5 mL toluene in a 20 mL scintillation vial charged with a magnetic stir bar. 56.0 mg O=PPh$_3$ (0.2 mmol) was dissolved in approximately 4 mL toluene and added to the (^{tBu}pyrpyrr$_2$)Fe(OEt$_2$) solution in the 20 mL scintillation vial dropwise. The vial containing the O=PPh$_3$ was rinsed with additional toluene until all solid material had fully dissolved and these washings were added to the reaction mixture. A gradual color change to a lighter shade of red was noted. The solution was stirred for one day at room temperature. The reaction mixture was concentrated to approximately 2 mL and 15 mL hexane was added. The toluene/hexane solution was stored at -35 °C for one day resulting in deposition of crystalline material onto the vial floor. The supernatant was decanted, and the crystalline material dried under vacuum prior to isolation (101.4 mg, 0.1322 mmol, 66.1% yield). Single crystals suitable for a X-Ray diffraction study could be grown by slow evaporation of a pentane solution of (^{tBu}pyrpyrr$_2$)Fe(OPPh$_3$) for one day at -35 °C. **^{1}H NMR**, (C_6D_6, 500 MHz, 298 K): δ = 122.14 (2H, -Ar-*H*$_{pyrrolyl}$/*meta*-Ar-*H*$_{pyridine}$), 93.75 (2H, -Ar-*H*$_{pyrrolyl}$/*meta*-Ar-*H*$_{pyridine}$), 21.56 (1H, *para*-Ar-*H*$_{pyridine}$), 17.55 (18H, -C(C*H*$_3$)$_3$), 6.88 (18H, -C(C*H*$_3$)$_3$), 5.76 (6H, *ortho*-Ar-*H*$_{O=PPh3}$/ *meta*-Ar-*H*$_{O=PPh3}$), 4.37 (3H, *para*-Ar-*H*$_{O=PPh3}$, -3.22 (6H, *ortho*-Ar-*H*$_{O=PPh3}$/ *meta*-Ar-*H*$_{O=PPh3}$). **Magnetic Moment**, (Evans' Method, C_6D_6, 500 MHz, 298 K): μ_{eff} = 4.8 μ_B. **UV-Vis**, toluene λ [nm ε (max/sh, $M^{-1}\cdot cm^{-1}$)]: 338 (max, 8550), 427 (max, 3780), 529 (sh, 907). **Elemental Analysis**: calculated for **1-O^{Ph}**: C, 73.72; H, 7.37; N, 5.49; found: C, 73.60; H, 7.37; N, 5.34.

3.2 Synthesis of (^{tBu}pyrpyrr$_2$)Fe(SPPh$_3$) (1-S^{Ph}). 112.2 mg (^{tBu}pyrpyrr$_2$)Fe(OEt$_2$) (0.2 mmol) was dissolved in 5 mL toluene in a 20 mL scintillation vial charged with a magnetic stir bar. 60.0 mg

S=PPh_3 (0.2 mmol) was dissolved in approximately 4 mL toluene and added to the (*t*Bupyrpyrr$_2$)Fe(OEt_2) solution in the 20 mL scintillation vial dropwise. The vial containing the S=PPh_3 was rinsed with additional toluene until all solid material had fully dissolved and these washings were added to the reaction mixture. A gradual color change to a lighter shade of red was noted. The solution was stirred for one day at room temperature and a small amount of material precipitated out of solution. The reaction mixture was concentrated to approximately 1 mL and 15 mL *n*-hexane was added resulting in significant precipitation of light red solid material. This light red solid was isolated on a frit (115.0 mg, 0.1471 mmol, 73.5% yield). Single crystals suitable for a X-Ray diffraction study could be grown by slow evaporation of *n*-hexane into a concentrated toluene solution of ($^{t\text{Bu}}$pyrpyrr$_2$)Fe($SPPh_3$) for one day followed by storage of this solution at -35 °C for one day. **^{1}H NMR**, (C_6D_6, 500 MHz, 298 K): δ = 117.15 (2H, -Ar-H_{pyrrolyl}/*meta*-Ar-H_{pyridine}), 103.65 (1H, *para*-Ar-H_{pyridine}), 23.11 (18H, -C(CH_3)$_3$), 16.83 (2H, -Ar-H_{pyrrolyl}/*meta*-Ar-H_{pyridine}), 8.70 (18H, -C(CH_3)$_3$), 4.74 (6H, *ortho*-Ar-$H_{\text{S=PPh3}}$), -2.05 (9H, *meta*,*para*-Ar-$H_{\text{S=PPh3}}$). Due to the poor solubility of ($^{t\text{Bu}}$pyrpyrr$_2$)Fe($SPPh_3$) in organic solvents a reliable solution state magnetic moment could not be measured. **UV-Vis**, toluene λ [nm ε (max/sh, $M^{-1}\cdot cm^{-1}$)]: 327 (max, 11300), 430 (max, 4640), 517 (sh, 1260). **Elemental Analysis,** calculated for **1-S$^{\text{Ph}}$**: C, 72.20; H, 7.22; N, 5.37; found: C, 70.95; H, 7.00; N, 5.32.

3.3 Synthesis of ($^{\text{tBu}}$pyrpyrr$_2$)Fe($SePPh_3$) (1-Se$^{\text{Ph}}$). 112.2 mg ($^{t\text{Bu}}$pyrpyrr$_2$)Fe(OEt_2) (0.2 mmol) was dissolved in 5 mL toluene in a 20 mL scintillation vial charged with a magnetic stir bar. 68.0 mg Se=PPh_3 (0.2 mmol) was dissolved in approximately 4 mL toluene and added to the ($^{t\text{Bu}}$pyrpyrr$_2$)Fe(OEt_2) solution in the 20 mL scintillation vial dropwise. The vial containing the Se=PPh_3 was rinsed with additional toluene until all solid material had fully dissolved and these washings were added to the reaction mixture. A gradual color change to a lighter shade of red was

noted. The solution was stirred for one day at room temperature and a small amount of material precipitated out of solution. The reaction mixture was concentrated to approximately 1 mL and 15 mL *n*-hexane was added resulting in significant precipitation of light red solid material. This light red solid was isolated on a frit (130.4 mg, 0.1574 mmol,78.7% yield). Single crystals suitable for a X-Ray diffraction study could be grown by slow evaporation of a methylene chloride solution of ($^{t\text{Bu}}$pyrpyrr$_2$)Fe(SePPh$_3$) at room temperature over 3 days. **^{1}H NMR**, (C_6D_6, 500 MHz, 298 K): δ = 115.17 (2H, -Ar-H_{pyrrolyl}/*meta*-Ar-H_{pyridine}), 102.54 (1H, *para*-Ar-H_{pyridine}), 23.69 (18H, -C(CH_3)$_3$), 16.53 (2H, -Ar-H_{pyrrolyl}/*meta*-Ar-H_{pyridine}), 9.36 (18H, -C(CH_3)$_3$), 6.87 (6H, *meta*-Ar-$H_{\text{Se=PPh3}}$), 4.83 (6H, *ortho*-Ar-$H_{\text{Se=PPh3}}$), -2.10 (3H, *para*-Ar-$H_{\text{Se=PPh3}}$). **Magnetic Moment**, (Evans' Method, C_6D_6, 500 MHz, 298 K): μ_{eff} = 4.4 μ_B. **UV-Vis**, toluene λ [nm ε (max/sh, $M^{-1}\cdot cm^{-1}$)]: 324 (max, 7050), 427 (max, 2410), 532 (sh, 29.8). **Elemental Analysis,** calculated for **1-Se$^{\text{Ph}}$**: C, 68.12; H, 6.81; N, 5.07; found: C, 67.53; H, 6.88; N, 5.04.

3.4 Synthesis of ($^{t\text{Bu}}$pyrpyrr$_2$)Fe(TeP^{t}Bu$_3$) (1-Te$^{t\text{Bu}}$). 112.2 mg ($^{t\text{Bu}}$pyrpyrr$_2$)Fe(OEt$_2$) (0.2 mmol) was dissolved in 5 mL toluene in a 20 mL scintillation vial charged with a magnetic stir bar. 66.0 mg Te=P^{t}Bu$_3$ (0.2 mmol) was dissolved in approximately 2 mL toluene and added to the ($^{t\text{Bu}}$pyrpyrr$_2$)Fe(OEt$_2$) solution in the 20 mL scintillation vial dropwise. A gradual color change to a lighter shade of red was noted. The solution was stirred for one day at room temperature and a significant amount of light red material precipitated out of solution. The reaction mixture was concentrated to approximately 1 mL and 15 mL *n*-hexane was added resulting in significant precipitation of light red solid material. This light red solid was isolated on a frit (125.1 mg, 0.1530 mmol,76.5% yield). Single crystals suitable for a X-Ray diffraction study could be grown by layering a toluene solution of ($^{t\text{Bu}}$pyrpyrr$_2$)Fe(TePPh$_3$) with pentane at room temperature for 2 days. **^{1}H NMR**, (C_6D_6, 500 MHz, 298 K): δ = 114.17 (2H, -Ar-H_{pyrrolyl}/*meta*-Ar-H_{pyridine}), 104.18

(1H, *para*-Ar-$H_{pyridine}$), 28.92 (18H, -C(CH_3)$_3$), 15.77 (2H, -Ar-$H_{pyrrolyl}$/*meta*-Ar-$H_{pyridine}$), 9.16 (18H, -C(CH_3)$_3$), -5.31 (27H, -C(CH$_3$)$_3$-*the*$_{=PtBu3}$). **Magnetic Moment**, (Evans' Method, C_6D_6, 500 MHz, 298 K): μ_{eff} = 4.9 μ_B. **UV-Vis**, toluene λ [nm ε (max/sh, $M^{-1}\cdot cm^{-1}$)]: 334 (max, 24300), 427 (max, 7930), 528 (sh, 37.0). **Elemental Analysis,** calculated for **1-Te^{tBu}**: C, 60.24; H, 8.39; N, 5.14; found: C, 59.42; H, 8.06; N, 5.16.

3.5 Synthesis of [K]$_2$[(^{tBu}pyrpyrr$_2$)Fe$_2$(μ-O)] (2-O). 108 mg [K]$_2$[($^{t\text{Bu}}$pyrpyrr$_2$)Fe$_2$(μ-N$_2$)] (0.1 mmol) was dissolved in 10 mL toluene in a 20 mL scintillation vial charged with a magnetic stir bar and the solution was chilled to -35 °C. 16 mg mesityl nitrile oxide (MesCNO, 0.1 mmol) was dissolved in 4 mL toluene and the solution was chilled to -35 °C. The MesCNO solution was added to the [K]$_2$[($^{t\text{Bu}}$pyrpyrr$_2$)Fe$_2$(μ-N$_2$)] solution dropwise while stirring, resulting in a color change to light orange. The reaction mixture was stirred for one day while slowly warming up to room temperature resulting in a light orange solution with a light orange precipitate. The reaction mixture was filtered through a celite plug supported on glass wool into a 20 mL scintillation vial and extracted with toluene until that vial was full. The remaining orange solid was extracted with another 80 mL toluene into four separate 20 mL scintillation vials. Each vial was concentrated to 2 mL and stored at -35 °C for one day. The contents of each of the five total vials was pipetted onto a glass frit and dried under vacuum to isolate the light orange microcrystalline product (67.5 mg, 0.063 mmol, 63.1% yield). Single crystals suitable for a X-Ray diffraction study were grown by slow evaporation of a diethyl ether solution of [K]$_2$[($^{t\text{Bu}}$pyrpyrr$_2$)Fe$_2$(μ-O)] over a period of four days at -35 °C. **^{1}H NMR**, (C_6D_6, 500 MHz, 298 K): δ = 32.01 (2H, -Ar-$H_{pyrrolyl}$/*meta*-Ar-$H_{pyridine}$), 19.84 (2H, -Ar-$H_{pyrrolyl}$/*meta*-Ar-$H_{pyridine}$), 2.96 (18H, -C(CH_3)$_3$), 2.49 (1H, *para*-Ar-$H_{pyridine}$), -0.68 (18H, -C(CH_3)$_3$). **Magnetic Moment**, (Evans' Method, C_6D_6, 500 MHz, 298 K): μ_{eff} = 3.5 μ_B. **UV-Vis**, toluene λ [nm ε (max/sh, $M^{-1}\cdot cm^{-1}$)]: 331 (max, 19700), 408 (max, 8300), 502 (sh, 1150).

Due to the air sensitivity of this compound satisfactory elemental analysis could not be obtained. The C, H, and N values were systematically low, despite inclusion of co-crystallized solvent molecules.

3.6 Synthesis of [K]$_2$[($^{t\text{Bu}}$pyrpyrr$_2$)Fe$_2$(μ-S)] (2-S). 108 mg [K]$_2$[(*t*Bupyrpyrr2)Fe$_2$(μ-N$_2$)] (0.1 mmol) was dissolved in 10 mL toluene in a 20 mL scintillation vial charged with a magnetic stir bar. 60.0 mg S=PPh$_3$ (0.1 mmol) was dissolved in 4 mL toluene. The S=PPh$_3$ solution was added to the [K]$_2$[($^{t\text{Bu}}$pyrpyrr$_2$)Fe$_2$(μ-N$_2$)] solution dropwise while stirring resulting in a color change to light red. The solution was stirred at room temperature for one day and some orange microcrystalline material precipitated out of solution. The reaction mixture was filtered through a celite plug supported on glass wool into a 20 mL scintillation vial and extracted with toluene until the vial was full. The remaining light orange solid was extracted with an additional 40 mL toluene and each of the three vials was concentrated to approximately 2 mL and stored at -35 °C for one day. The contents of each of the three vials was pipetted onto a glass frit and dried under vacuum to isolate the light orange microcrystalline product (71.8 mg, 0.066 mmol, 66.2% yield). Single crystals suitable for a X-Ray diffraction study could were grown by slow evaporation of a diethyl ether solution of [K]$_2$[($^{t\text{Bu}}$pyrpyrr$_2$)Fe$_2$(μ-S)] at -35 °C over a period of 4 days. **^{1}H NMR**, (C$_6$D$_6$, 500 MHz, 298 K): δ = 46.91 (2H, -Ar-*H*$_{\text{pyrrolyl}}$/*meta*-Ar-*H*$_{\text{pyridine}}$), 35.20 (2H, -Ar-*H*$_{\text{pyrrolyl}}$/*meta*-Ar-*H*$_{\text{pyridine}}$), 6.87 (1H, *para*-Ar-*H*$_{\text{pyridine}}$), -2.31 (18H, -C(C*H*$_3$)$_3$), -6.89 (18H, -C(C*H*$_3$)$_3$). **Magnetic Moment**, (Evans' Method, C$_6$D$_6$, 500 MHz, 298 K): μ_{eff} = 5.5 μ_B. **UV-Vis**, toluene λ [nm ε (max/sh, M^{-1}·cm^{-1})]: 324 (max, 33700), 398 (max, 12100), 496 (sh, 795). **Elemental Analysis,** calculated for **2-O·0.5 tol**: C, 65.29; H, 7.62; N, 7.43; found: C, 64.48; H, 7.37; N, 7.35.

3.7 Synthesis of [K]$_2$[($^{t\text{Bu}}$pyrpyrr$_2$)Fe$_2$(μ-Se)] (2-Se). 108 mg [K]$_2$[($^{t\text{Bu}}$pyrpyrr$_2$)Fe$_2$(μ-N$_2$)] (0.1 mmol) was dissolved in 10 mL toluene in a 20 mL scintillation vial charged with a magnetic stir

bar. 68.0 mg Se=PPh_3 (0.1 mmol) was dissolved in 4 mL toluene. The Se=PPh_3 solution was added to the $[K]_2[(^{tBu}pyrpyrr_2)Fe_2(\mu\text{-}N_2)]$ solution dropwise while stirring resulting in a color change to dark red. The vial containing Se=PPh_3 was washed with more toluene and the washings added to the reaction solution until all the Se=PPh_3 was dissolved. The solution was stirred at room temperature for one day resulting in a rapid color change to red. The reaction mixture was filtered through a celite plug supported on glass wool into a 20 mL scintillation vial. An additional 2 mL toluene was washed through the celite plug. The filtered toluene solution was concentrated to approximately 2 mL and stored at -35 °C for one day resulting in the formation of light red crystalline material. The supernatant was decanted and the crystalline solid dried under vacuum prior to isolation (74.5 mg, 0.066 mmol, 65.8% yield). Single crystals suitable for a X-Ray diffraction study were grown by slow evaporation of a diethyl ether solution of $[K]_2[(^{tBu}pyrpyrr_2)Fe_2(\mu\text{-}Se)]$ at -35 °C over a period of 4 days. **^{1}H NMR**, (C_6D_6, 500 MHz, 298 K): δ = 58.38 (2H, -Ar-$H_{pyrrolyl}$/*meta*-Ar-$H_{pyridine}$), 48.81 (2H, -Ar-$H_{pyrrolyl}$/*meta*-Ar-$H_{pyridine}$), 8.54 (1H, *para*-Ar-$H_{pyridine}$), -0.61 (18H, -C(CH_3)$_3$), -4.85 (18H, -C(CH_3)$_3$). **Magnetic Moment**, (Evans' Method, C_6D_6, 500 MHz, 298 K): μ_{eff} = 5.3 μ_B. **UV-Vis**, toluene λ [nm ε (max/sh, $M^{-1}\cdot cm^{-1}$)]: 324 (max, 10200), 399 (max, 3750), 509 (sh, 214). **Elemental Analysis,** calculated for **2-Se·2 tol**: C, 65.69; H, 7.50; N, 6.38; found: C, 65.25; H, 7.44; N, 6.40.

3.8 Synthesis of $[K]_2[(^{tBu}pyrpyrr_2)Fe_2(\mu\text{-}Te)]$ (2-Te). 108 mg $[K]_2[(^{tBu}pyrpyrr)_2Fe_2(\mu\text{-}N_2)]$ (0.1 mmol) was dissolved in 10 mL toluene in a 20 mL scintillation vial charged with a magnetic stir bar. 33.0 mg Te=P^{t}Bu$_3$ (0.1 mmol) was dissolved in 4 mL toluene. The Te=P^{t}Bu$_3$ solution was added to the $[K]_2[(^{tBu}pyrpyrr_2)Fe_2(\mu\text{-}N_2)]$ solution dropwise while stirring resulting in a color change to dark red. The solution was stirred at room temperature for one day. The reaction mixture was filtered through a celite plug supported on glass wool into a 20 mL scintillation vial. The celite

plug was washed with an additional 2 mL toluene and the filtered solution was concentrated to approximately 2 mL and stored at -35 °C for one day resulting in the formation of crystalline material. The supernatant was decanted, and the crystalline material was dried under vacuum prior to isolation (74.2 mg, 0.063 mmol, 62.8% yield). Single crystals suitable for a X-Ray diffraction study could be grown by slow evaporation of a diethyl ether solution of $[K]_2[(^{tBu}pyrpyrr_2)Fe_2(\mu\text{-}Te)]$ at -35 °C over a period of 4 days. **^{1}H NMR**, (C_6D_6, 500 MHz, 298 K): δ = 72.01 (2H, -Ar-$H_{pyrrolyl}$/*meta*-Ar-$H_{pyridine}$), 66.57 (2H, -Ar-$H_{pyrrolyl}$/*meta*-Ar-$H_{pyridine}$), 10.81 (1H, *para*-Ar-$H_{pyridine}$), 2.46 (18H, -C(CH_3)$_3$), 0.42 (18H, -C(CH_3)$_3$). **Magnetic Moment**, (Evans' Method, C_6D_6, 500 MHz, 298 K): μ_{eff} = 5.9 μ_B. **UV-Vis**, toluene λ [nm ε (max/sh, $M^{-1}\cdot cm^{-1}$)]: 326 (max, 19700), 404 (max, 8690), 502 (sh, 792). **Elemental Analysis,** calculated for **2-Te·1.5 tol**: C, 62.38; H, 7.18; N, 6.37; found: C, 59.25; H, 7.12; N, 6.37.

4 ^{1}H NMR Spectroscopy

4.1 ^{1}H NMR Spectrum of ($^{t\mathrm{Bu}}$pyrpyrr$_2$)Fe(OPPh$_3$) (1-O$^{\mathrm{Ph}}$)

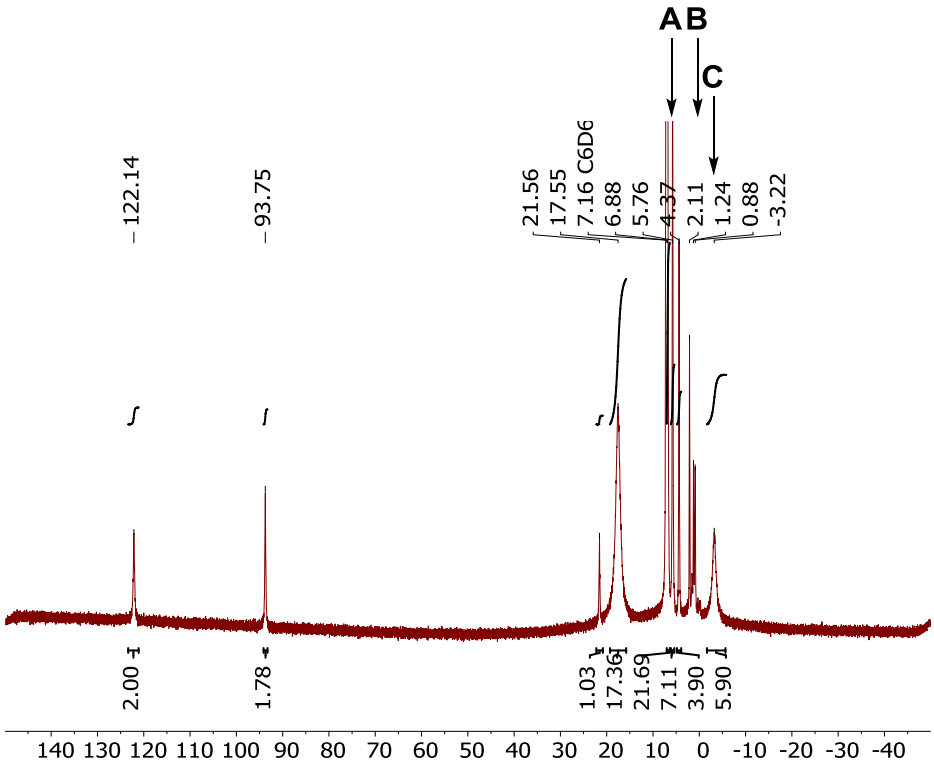

Figure S1. ^{1}H NMR spectrum of ($^{t\mathrm{Bu}}$pyrpyrr$_2$)Fe(OPPh$_3$) (**1-O$^{\mathrm{Ph}}$**) (C_6D_6, 500 MHz, 298 K). Visible impurities are labeled as follows: **A** = C_6H_6 ($\delta = 7.16$), **B** = toluene ($\delta = 2.11$), **C** = hexane ($\delta = 1.24$, 0.88).

4.2 ^{1}H NMR Spectrum of ($^{t\text{Bu}}$pyrpyrr$_2$)Fe(SPPh$_3$) (1-S^{Ph})

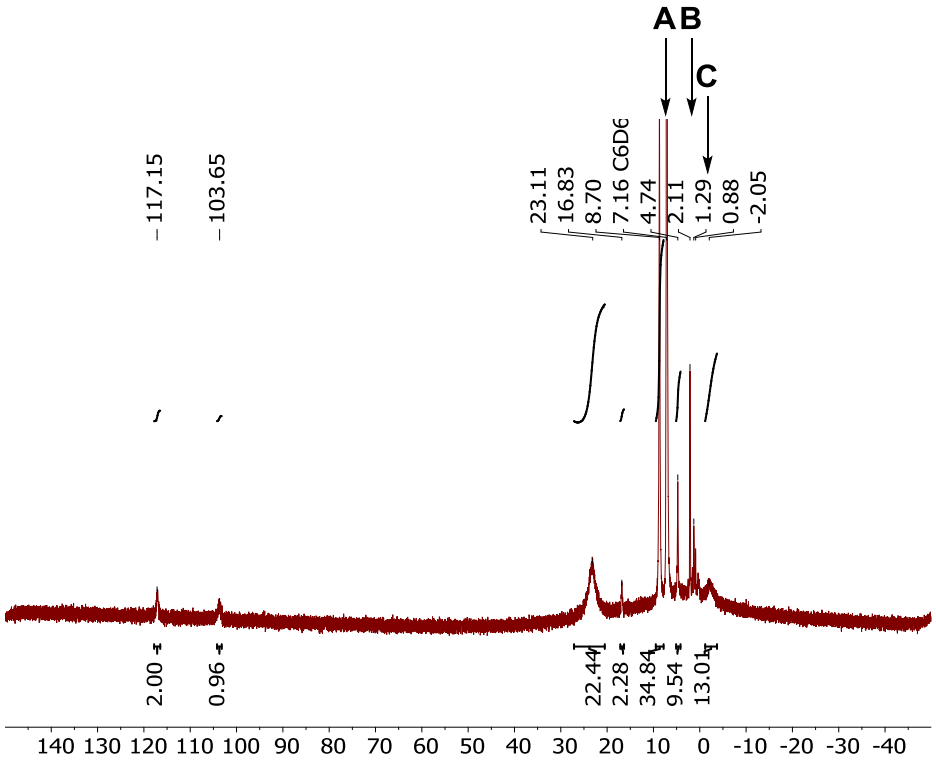

Figure S2. ^{1}H NMR spectrum of ($^{t\text{Bu}}$pyrpyrr$_2$)Fe(SPPh$_3$) (**1-S^{Ph}**) (C_6D_6, 500 MHz, 298 K). Visible impurities are labeled as follows: **A** = C_6H_6 ($\delta = 7.16$), **B** = toluene ($\delta = 2.11$), **C** = hexane ($\delta = 1.29, 0.88$).

4.3 ^{1}H NMR Spectrum of ($^{t\mathrm{Bu}}$pyrpyrr$_2$)Fe(SePPh$_3$) (1-Se$^{\mathrm{Ph}}$)

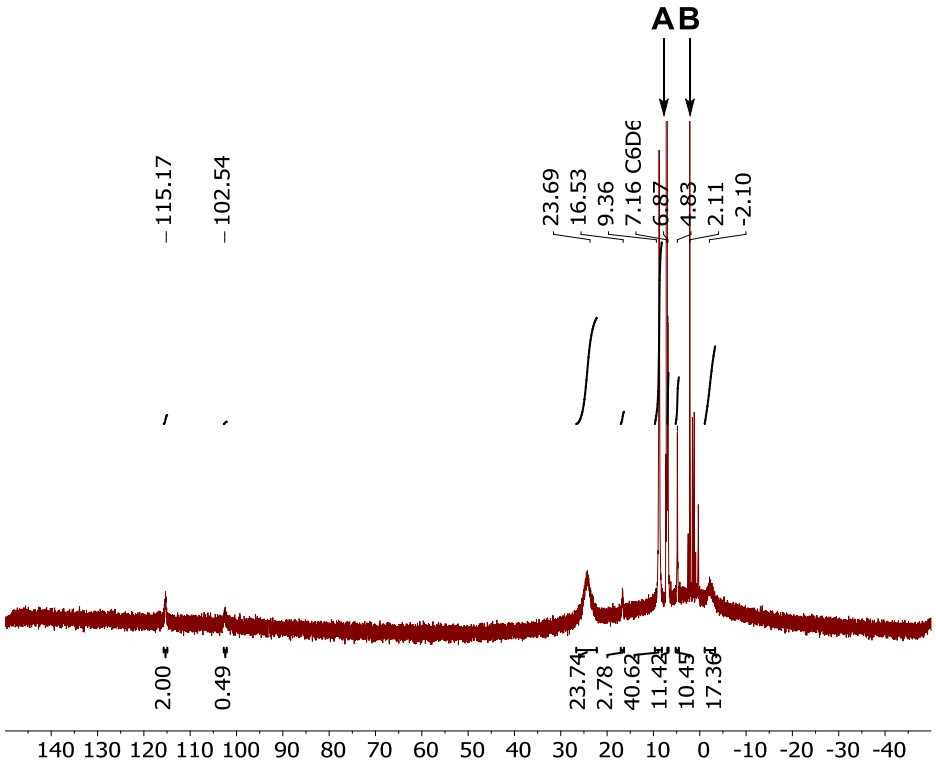

Figure S3. ^{1}H NMR spectrum of ($^{t\mathrm{Bu}}$pyrpyrr$_2$)Fe(SePPh$_3$) (**1-Se$^{\mathrm{Ph}}$**) (C_6D_6, 500 MHz, 298 K). Visible impurities are labeled as follows: **A** = C_6H_6 ($\delta = 7.16$), **B** = toluene ($\delta = 2.11$). *Due to insolubility and paramagnetism of **1-Se$^{\mathrm{Ph}}$** in C_6D_6 integrations may not be accurate.*

4.4 ^{1}H NMR Spectrum of (^{tBu}pyrpyrr$_2$)Fe(TeP^{t}Bu$_3$) (1-Te^{tBu})

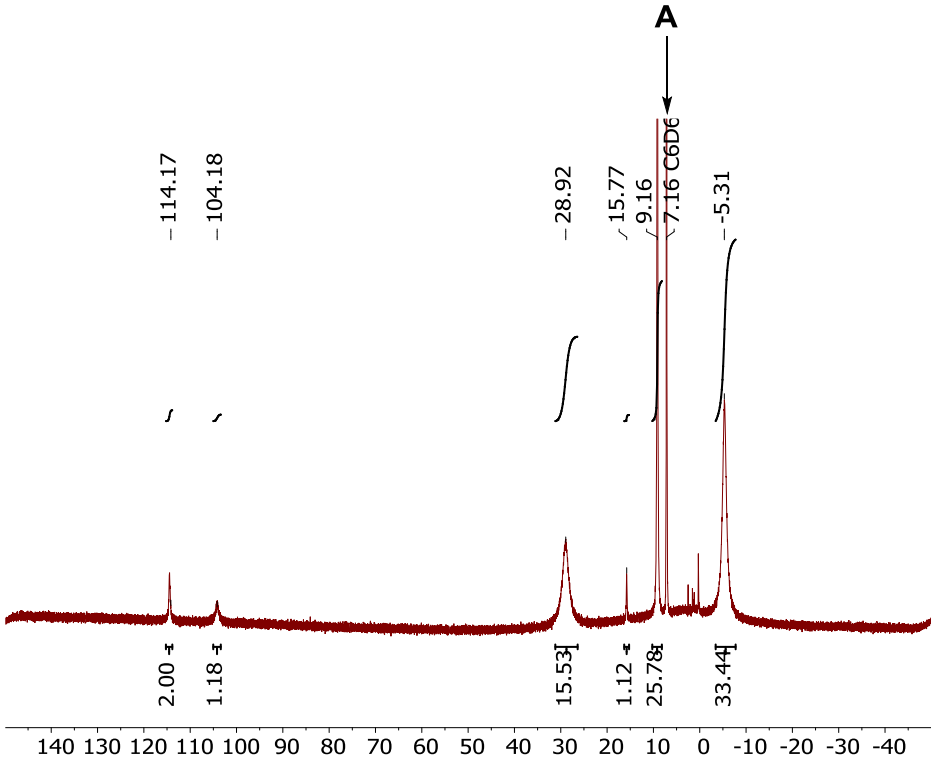

Figure S4. ^{1}H NMR spectrum of (^{tBu}pyrpyrr$_2$)Fe(TeP^{t}Bu$_3$) (**1-Te^{tBu}**) (C_6D_6, 500 MHz, 298 K). Visible impurities are labeled as follows: **A** = C_6H_6 (δ = 7.16).

4.5 ^{1}H NMR Spectrum of $[K]_2[(^{tBu}pyrpyrr_2)Fe_2(\mu\text{-}O)]$ (2-O)

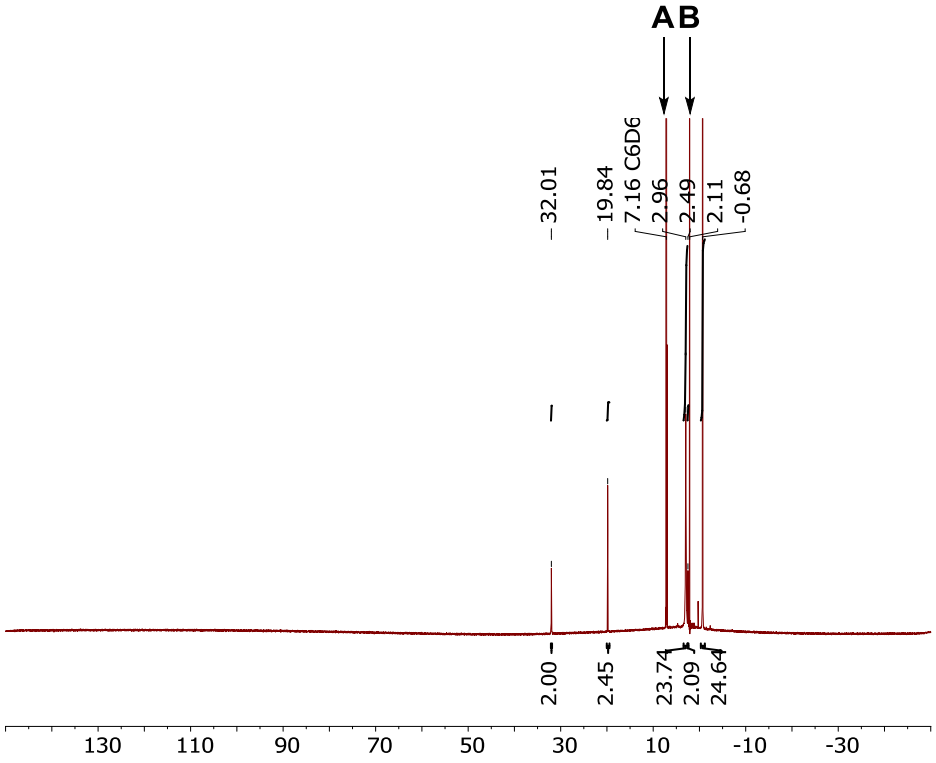

Figure S5. ^{1}H NMR spectrum of $[K]_2[(^{tBu}pyrpyrr_2)Fe_2(\mu\text{-}O)]$ (**2-O**) (C_6D_6, 500 MHz, 298 K). Visible impurities are labeled as follows: **A** = C_6H_6 ($\delta = 7.16$), **B** = toluene ($\delta = 2.11$).

4.6 ^{1}H NMR Spectrum of $[K]_2[(^{tBu}pyrpyrr_2)Fe_2(\mu\text{-}S)]$ (2-S)

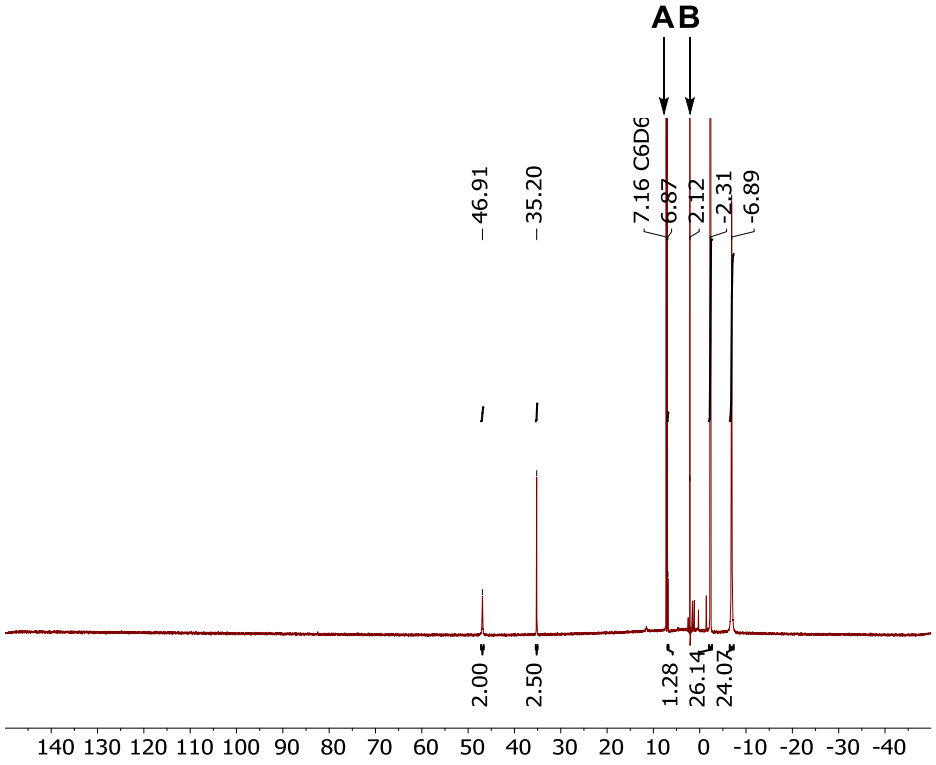

Figure S6. ^{1}H NMR spectrum of $[K]_2[(^{tBu}pyrpyrr_2)Fe_2(\mu\text{-}S)]$ (**2-S**) (C_6D_6, 500 MHz, 298 K). Visible impurities are labeled as follows: **A** = C_6H_6 ($\delta = 7.16$), **B** = toluene ($\delta = 2.11$).

4.7 ^{1}H NMR Spectrum of [K]$_2$[($^{t\text{Bu}}$pyrpyrr$_2$)Fe$_2$(μ-Se)] (2-Se)

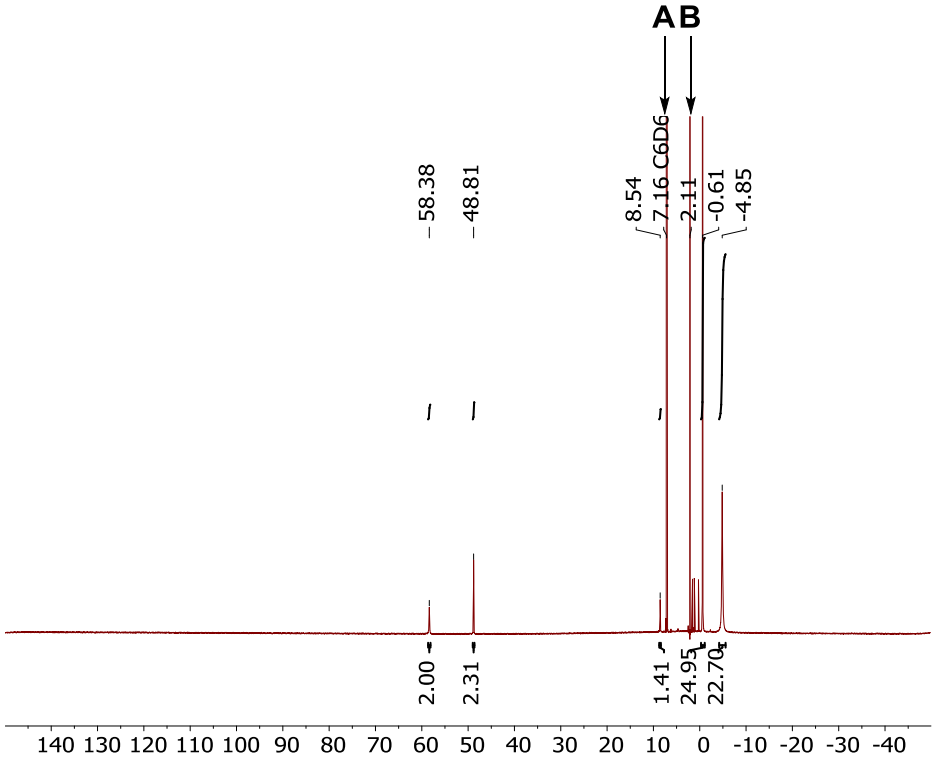

Figure S7. ^{1}H NMR spectrum of [K]$_2$[($^{t\text{Bu}}$pyrpyrr$_2$)Fe$_2$(μ-Se)] (**2-Se**) (C_6D_6, 500 MHz, 298 K). Visible impurities are labeled as follows: **A** = C_6H_6 (δ = 7.16), **B** = toluene (δ = 2.11).

4.8 ^{1}H NMR Spectrum of [K]$_2$[($^{t\text{Bu}}$pyrpyrr$_2$)Fe$_2$(μ-Te)] (2-Te)

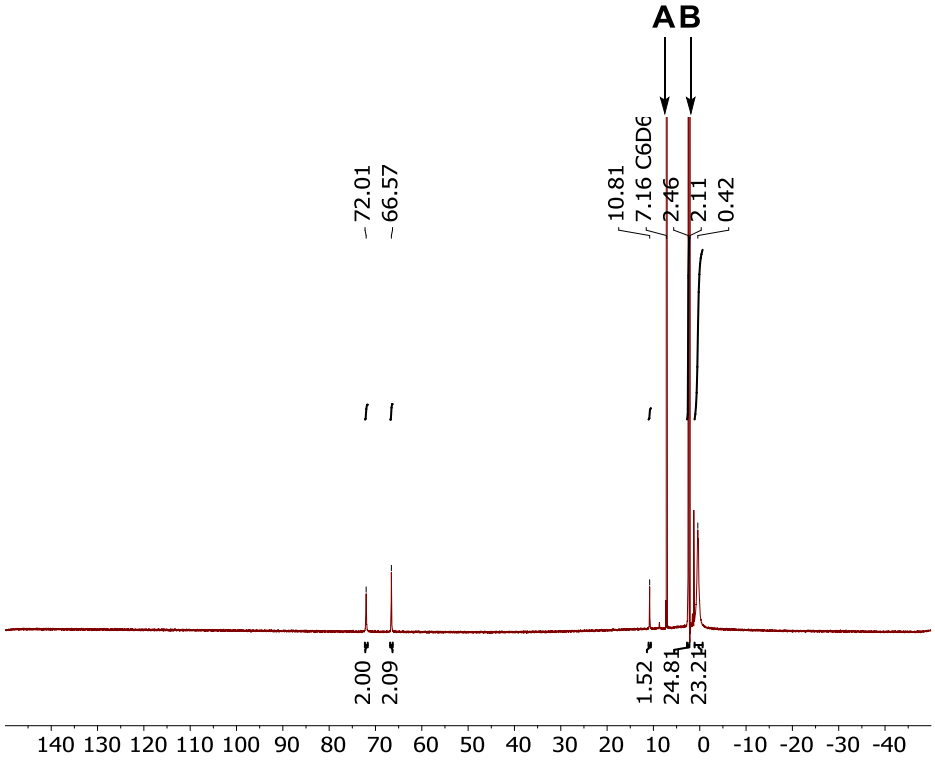

Figure S8. ^{1}H NMR spectrum of [K]$_2$[($^{t\text{Bu}}$pyrpyrr$_2$)Fe$_2$(μ-Te)] (**2-Te**) (C_6D_6, 500 MHz, 298 K). Visible impurities are labeled as follows: **A** = C_6H_6 (δ = 7.16), **B** = toluene (δ = 2.11).

5 UV-Vis Spectroscopy

5.1 UV-Vis Spectrum of ($^{t\mathrm{Bu}}$pyrpyrr$_2$)Fe(OPPh$_3$) (**1-O$^{\mathrm{Ph}}$**)

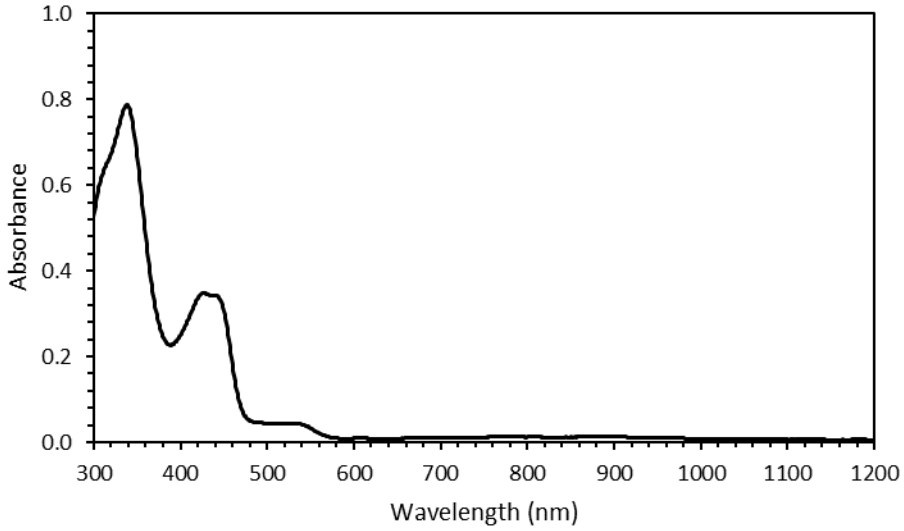

Figure S9. UV-Vis spectrum of ($^{t\mathrm{Bu}}$pyrpyrr$_2$)Fe(OPPh$_3$) (**1-O$^{\mathrm{Ph}}$**) in toluene at 298 K. [**1-O$^{\mathrm{Ph}}$**] = $4.94 \cdot 10^{-5}$ mol·L^{-1}.

5.2 UV-Vis Spectrum of ($^{t\mathrm{Bu}}$pyrpyrr$_2$)Fe(SPPh$_3$) (**1-S$^{\mathrm{Ph}}$**)

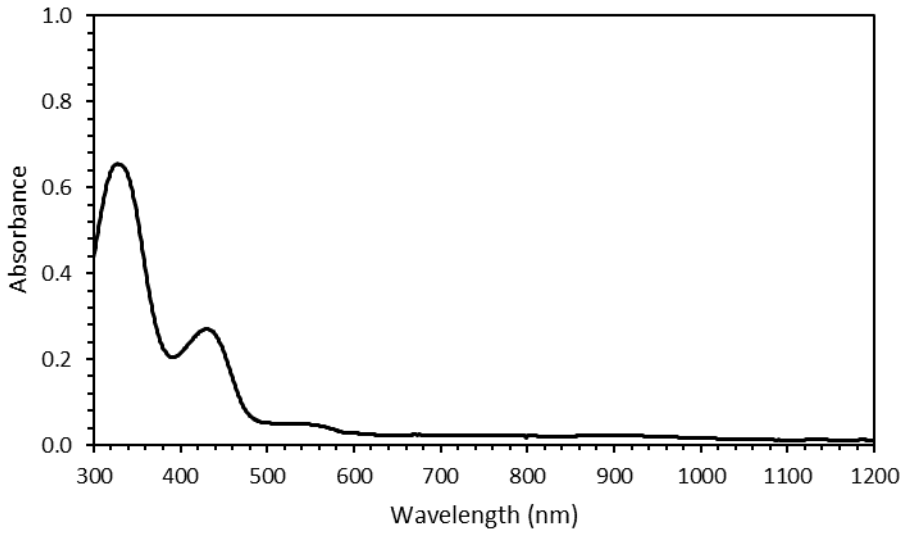

Figure S10. UV-Vis spectrum of ($^{t\mathrm{Bu}}$pyrpyrr$_2$)Fe(SPPh$_3$) (**1-S$^{\mathrm{Ph}}$**) in toluene at 298 K. [**1-S$^{\mathrm{Ph}}$**] = $3.98 \cdot 10^{-5}$ mol·L^{-1}.

5.3 UV-Vis Spectrum of ($^{t\mathrm{Bu}}$pyrpyrr$_2$)Fe(SePPh$_3$) (**1-Se$^{\mathrm{Ph}}$**)

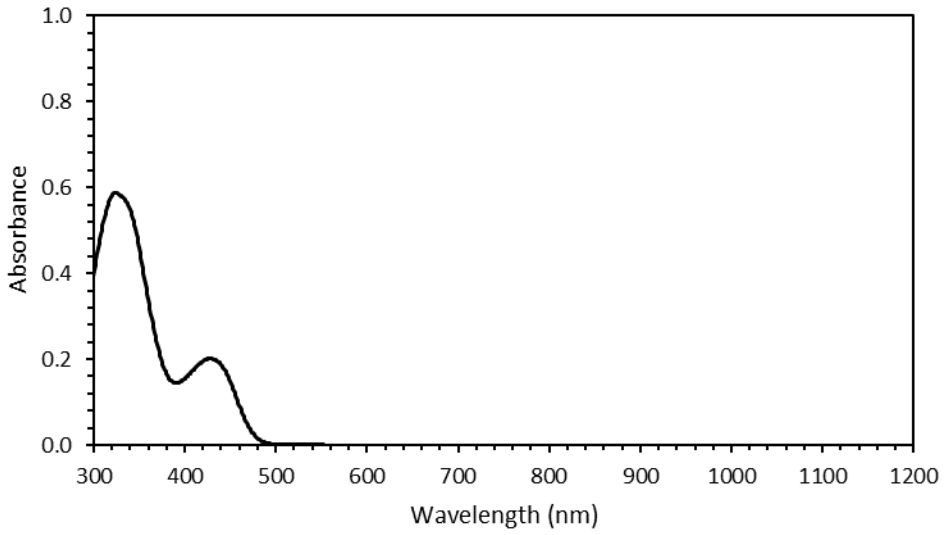

Figure S11. UV-Vis spectrum of ($^{t\mathrm{Bu}}$pyrpyrr$_2$)Fe(SePPh$_3$) (**1-Se$^{\mathrm{Ph}}$**) in toluene at 298 K. [**1-Se$^{\mathrm{Ph}}$**] = $8.340 \cdot 10^{-5}$ mol·L^{-1}.

5.4 UV-Vis Spectrum of ($^{t\mathrm{Bu}}$pyrpyrr$_2$)Fe(TeP^{t}Bu$_3$) (**1-Te$^{t\mathrm{Bu}}$**)

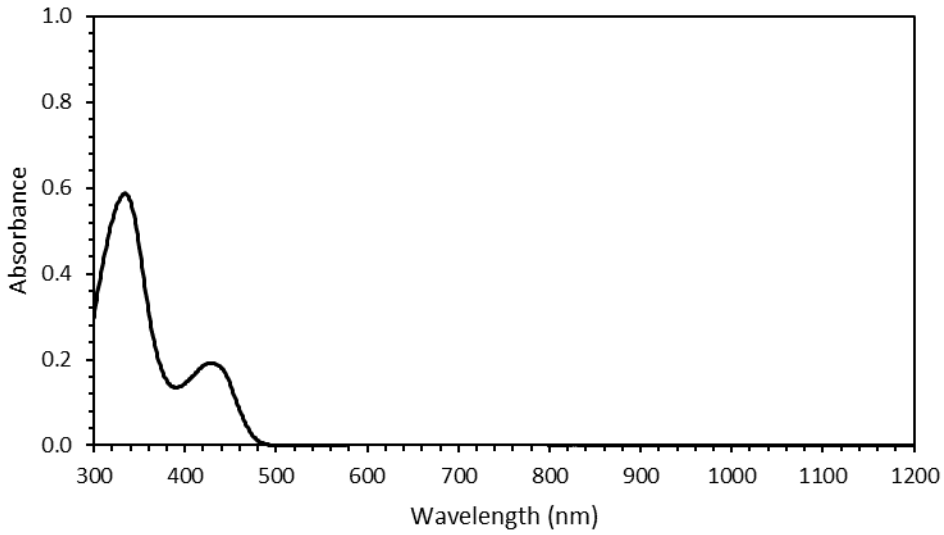

Figure S12. UV-Vis spectrum of ($^{t\mathrm{Bu}}$pyrpyrr$_2$)Fe(TeP^{t}Bu$_3$) (**1-Te$^{t\mathrm{Bu}}$**) in toluene at 298 K. [**1-Te$^{t\mathrm{Bu}}$**] = $2.42 \cdot 10^{-5}$ mol·L^{-1}.

5.5 UV-Vis Spectrum of $[K]_2[(^{tBu}pyrpyrr_2)Fe_2(\mu\text{-}O)]$ (2-O)

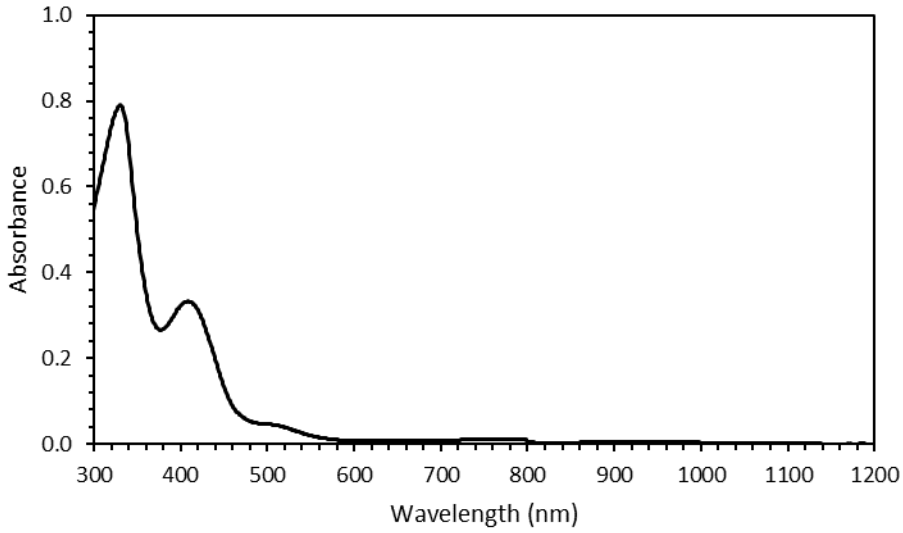

Figure S13. UV-Vis spectrum of $[K]_2[(^{tBu}pyrpyrr_2)Fe_2(\mu\text{-}O)]$ (**2-O**) in toluene at 298 K. [**2-O**] = $4.01 \cdot 10^{-5}$ mol·L^{-1}.

5.6 UV-Vis Spectrum of $[K]_2[(^{tBu}pyrpyrr_2)Fe_2(\mu\text{-}S)]$ (2-S)

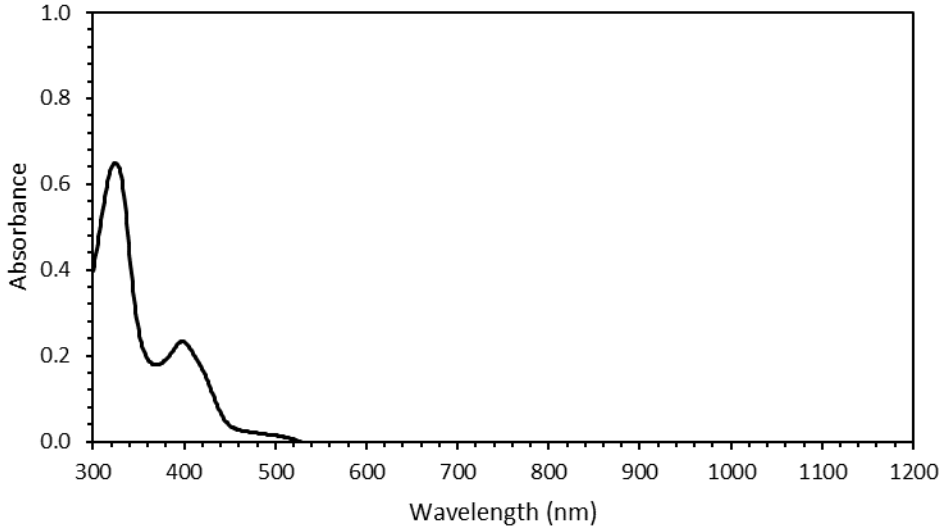

Figure S14. UV-Vis spectrum of $[K]_2[(^{tBu}pyrpyrr_2)Fe_2(\mu\text{-}S)]$ (**2-S**) in toluene at 298 K. [**2-S**] = $1.93 \cdot 10^{-5}$ mol·L^{-1}.

5.7 UV-Vis Spectrum of $[K]_2[(^{tBu}pyrpyrr_2)Fe_2(\mu\text{-}Se)]$ (2-Se)

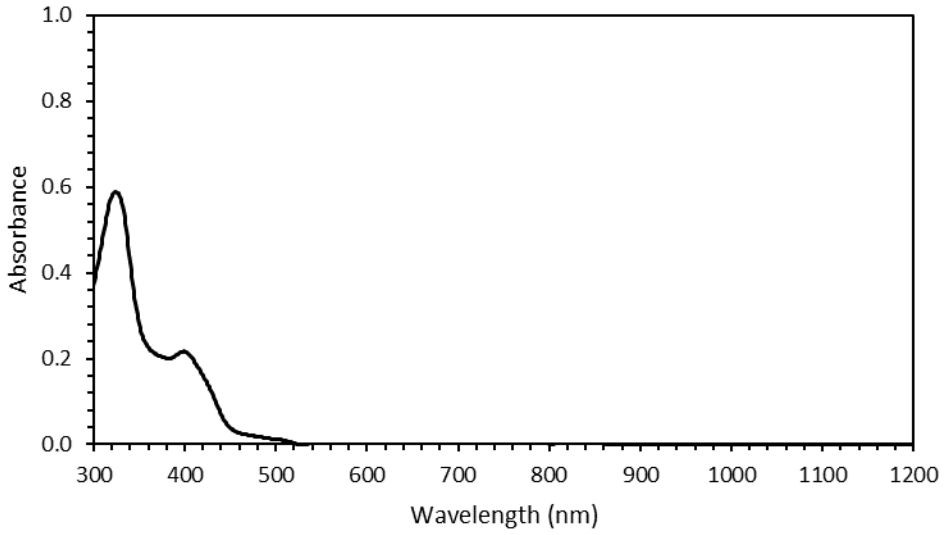

Figure S15. UV-Vis spectrum of $[K]_2[(^{tBu}pyrpyrr_2)Fe_2(\mu\text{-}Se)]$ (**2-Se**) in toluene at 298 K. [**2-Se**] = $5.78 \cdot 10^{-5}$ mol·L^{-1}.

5.8 UV-Vis Spectrum of $[K]_2[(^{tBu}pyrpyrr_2)Fe_2(\mu\text{-}Te)]$ (2-Te)

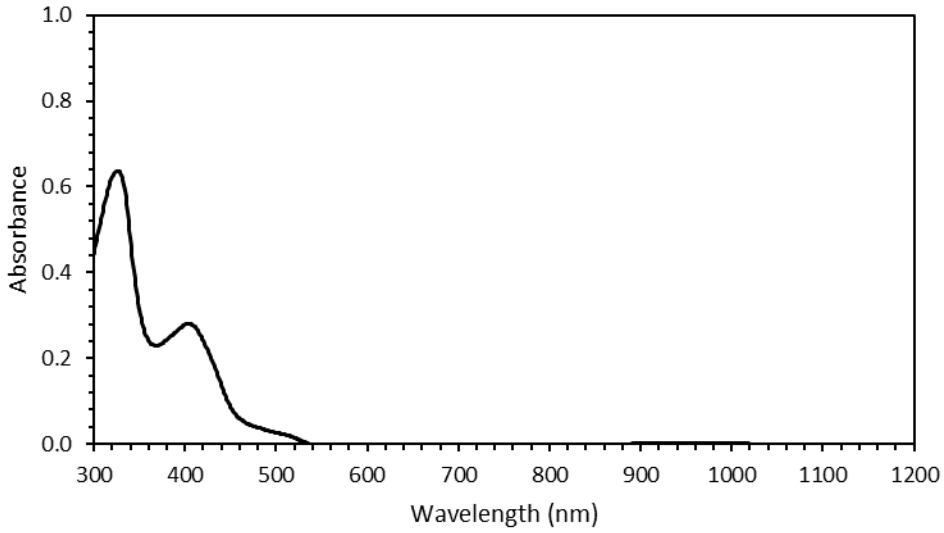

Figure S16. UV-Vis spectrum of $[K]_2[(^{tBu}pyrpyrr_2)Fe_2(\mu\text{-}Te)]$ (**2-Te**) in toluene at 298 K. [**2-Te**] = $3.24 \cdot 10^{-5}$ mol·L^{-1}.

6 Mossbauer Spectroscopy

6.1 Mössbauer Spectrum of (^{tBu}pyrpyrr$_2$)Fe(OPPh$_3$) (1-O^{Ph})

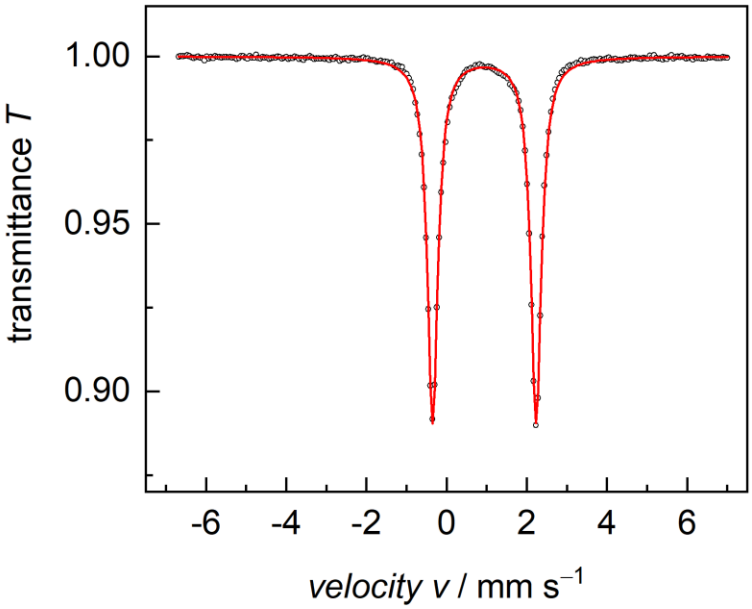

Figure S17. Zero-field ^{57}Fe Mössbauer spectrum of (^{tBu}pyrpyrr$_2$)Fe(OPPh$_3$) (**1-O^{Ph}**) recorded at 77 K. δ = 0.94 mm·s^{-1}, ΔE_Q = 2.58 mm·s^{-1}, Γ_{fwhm} = 0.32 mm·s^{-1}.

6.2 Mössbauer Spectrum of (^{tBu}pyrpyrr$_2$)Fe(SPPh$_3$) (1-S^{Ph})

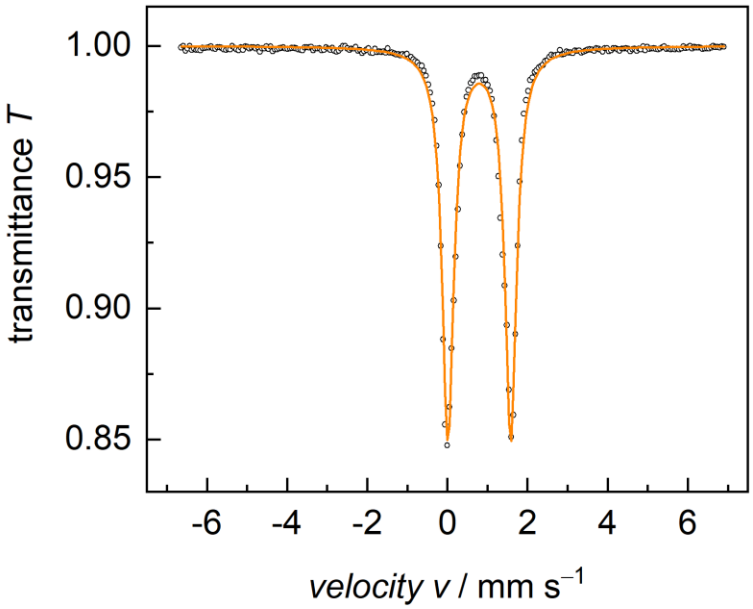

Figure S18. Zero-field ^{57}Fe Mössbauer spectrum of (^{tBu}pyrpyrr$_2$)Fe(SPPh$_3$) (**1-S^{Ph}**) recorded at 77 K. δ = 0.80 mm·s^{-1}, ΔE_Q = 1.57 mm·s^{-1}, Γ_{fwhm} = 0.35 mm·s^{-1}.

6.3 Mössbauer Spectrum of (^{tBu}pyrpyrr$_2$)Fe(SePPh$_3$) (1-Se^{Ph})

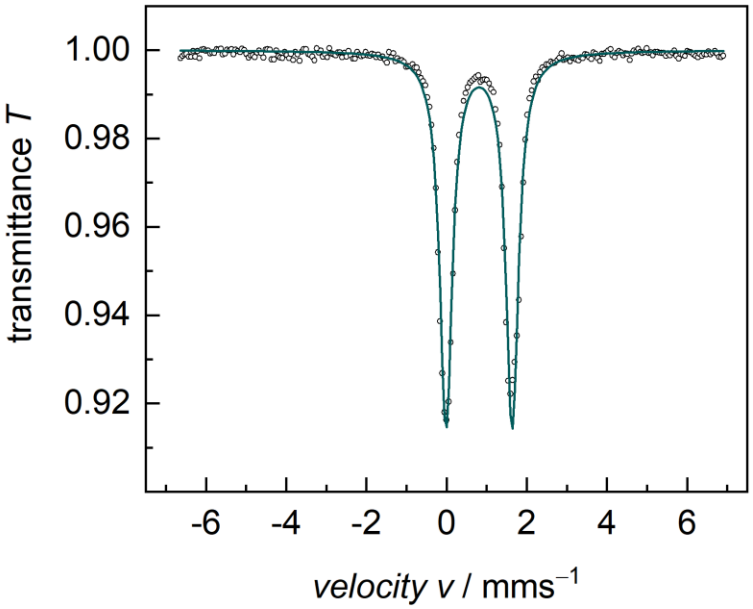

Figure S19. Zero-field ^{57}Fe Mössbauer spectrum of ($^{t\text{Bu}}$pyrpyrr$_2$)Fe(SePPh$_3$) (**1-Se^{Ph}**) recorded at 77 K. δ = 0.81 mm·s^{-1}, ΔE_Q = 1.65 mm·s^{-1}, Γ_{fwhm} = 0.38 mm·s^{-1}.

6.4 Mössbauer Spectrum of ($^{t\mathrm{Bu}}$pyrpyrr$_2$)Fe(TeP^{t}Bu$_3$) (**1-Te$^{t\mathrm{Bu}}$**)

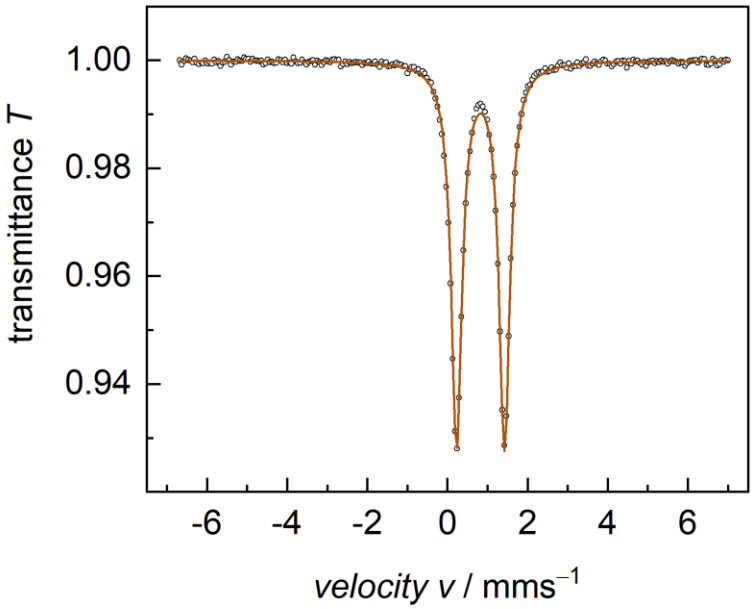

Figure S20. Zero-field ^{57}Fe Mössbauer spectrum of ($^{t\mathrm{Bu}}$pyrpyrr$_2$)Fe(TeP^{t}Bu$_3$) (**1-Te$^{t\mathrm{Bu}}$**) recorded at 77 K. δ = 0.82 mm·s^{-1}, ΔE_Q = 1.20 mm·s^{-1}, Γ_fwhm = 0.33 mm·s^{-1}.

6.5 Mössbauer Spectrum of $[K]_2[(^{tBu}pyrpyrr_2)Fe_2(\mu\text{-}O)]$ (2-O)

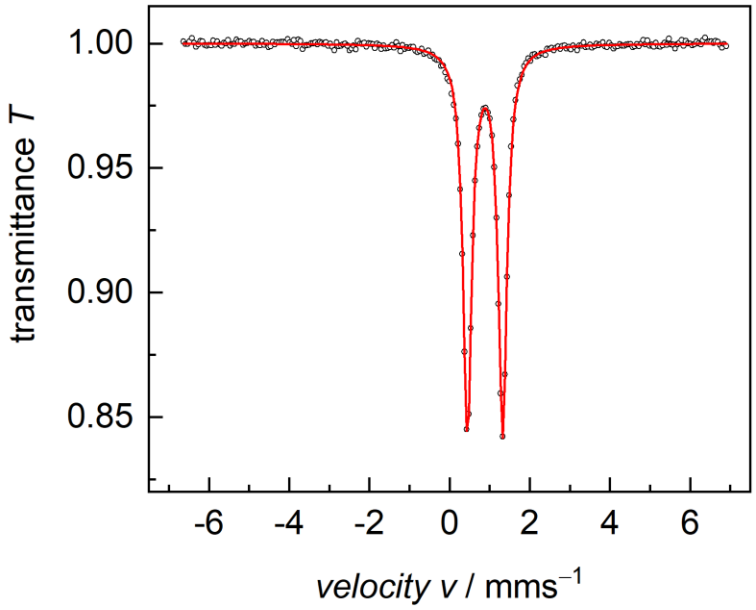

Figure S21. Zero-field ^{57}Fe Mössbauer spectrum of $[K]_2[(^{tBu}pyrpyrr_2)Fe_2(\mu\text{-}O)]$ (**2-O**) recorded at 77 K. $\delta = 0.88$ mm·s^{-1}, $\Delta E_Q = 0.88$ mm·s^{-1}, $\Gamma_{fwhm} = 0.26$ mm·s^{-1}.

6.6 Mössbauer Spectrum of $[K]_2[(^{tBu}pyrpyrr_2)Fe_2(\mu\text{-}S)]$ (2-S)

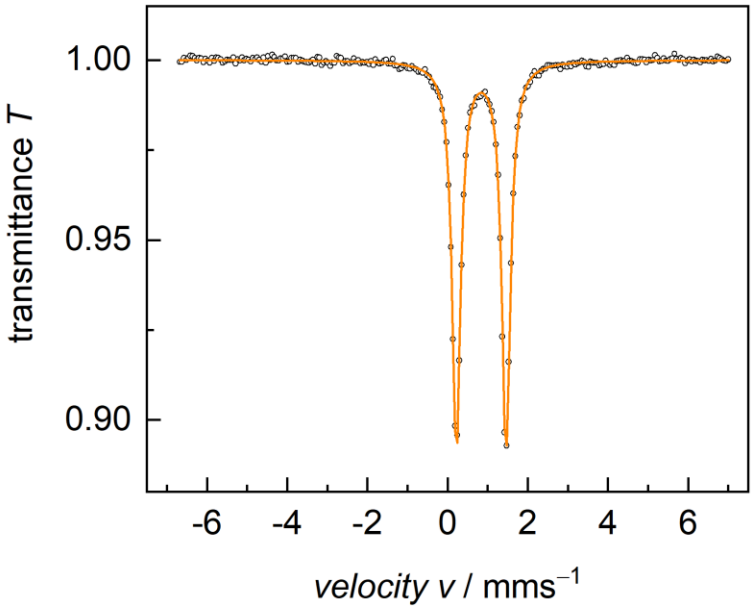

Figure S22. Zero-field ^{57}Fe Mössbauer spectrum of $[K]_2[(^{tBu}pyrpyrr_2)Fe_2(\mu\text{-}S)]$ (**2-S**) recorded at 77 K. $\delta = 0.84$ mm·s^{-1}, $\Delta E_Q = 1.24$ mm·s^{-1}, $\Gamma_{fwhm} = 0.26$ mm·s^{-1}.

6.7 Mössbauer Spectrum of $[K]_2[(^{tBu}pyrpyrr_2)Fe_2(\mu\text{-}Se)]$ (2-Se)

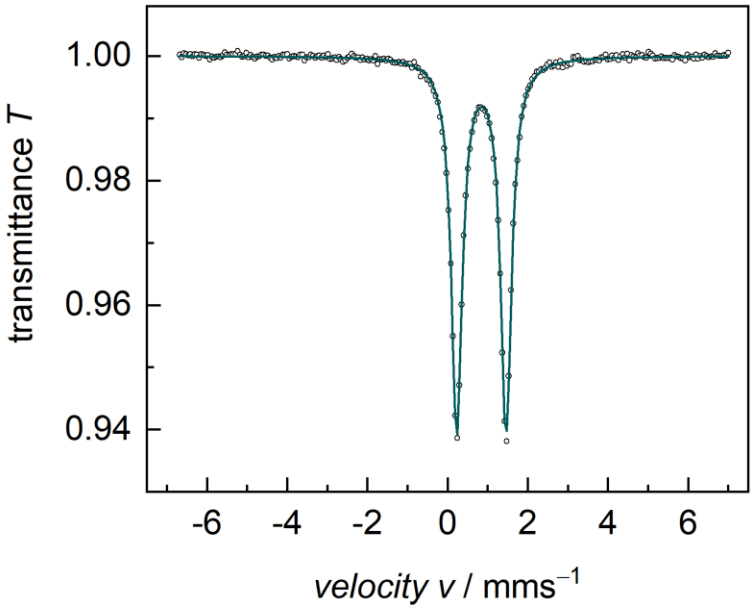

Figure S23. Zero-field ^{57}Fe Mössbauer spectrum of $[K]_2[(^{tBu}pyrpyrr_2)Fe_2(\mu\text{-}Se)]$ (**2-Se**) recorded at 77 K. $\delta = 0.84$ mm·s^{-1}, $\Delta E_Q = 1.23$ mm·s^{-1}, $\Gamma_{fwhm} = 0.33$ mm·s^{-1}.

6.8 Mössbauer Spectrum of $[K]_2[(^{tBu}pyrpyrr_2)Fe_2(\mu\text{-}Te)]$ (2-Te)

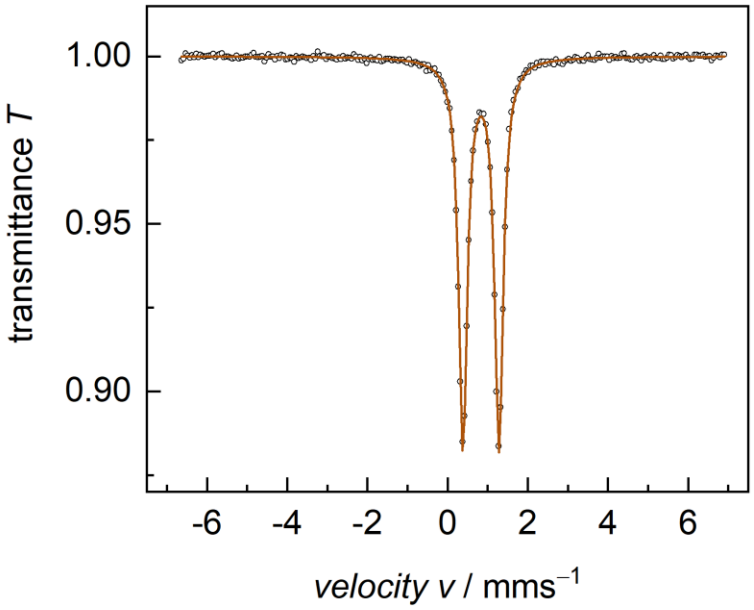

Figure S24. Zero-field ^{57}Fe Mössbauer spectrum of $[K]_2[(^{tBu}pyrpyrr_2)Fe_2(\mu\text{-}Te)]$ (**2-Te**) recorded at 77 K. $\delta = 0.83$ mm·s^{-1}, $\Delta E_Q = 0.90$ mm·s^{-1}, $\Gamma_{fwhm} = 0.26$ mm·s^{-1}.

7 SQUID Magnetometry

7.1 SQUID Plot of ($^{t\mathrm{Bu}}$pyrpyrr$_2$)Fe(OPPh$_3$) (1-O$^{\mathrm{Ph}}$) Sample 1

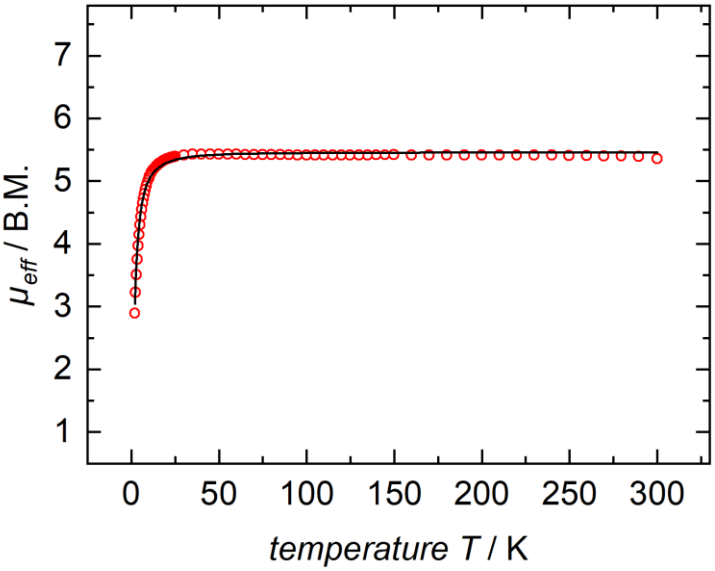

Figure S25. SQUID DC Field measurement at 1 T, 300-2 K, for ($^{t\mathrm{Bu}}$pyrpyrr$_2$)Fe(OPPh$_3$) (**1-O$^{\mathrm{Ph}}$**) sample 1 (33.9 mg, circles). The best fit (solid line) was obtained with $g_{\mathrm{av}} = 2.23$ and $|D| = 8$ cm^{-1}.

7.2 SQUID Plot of ($^{t\mathrm{Bu}}$pyrpyrr$_2$)Fe(OPPh$_3$) (1-O$^{\mathrm{Ph}}$) Sample 2

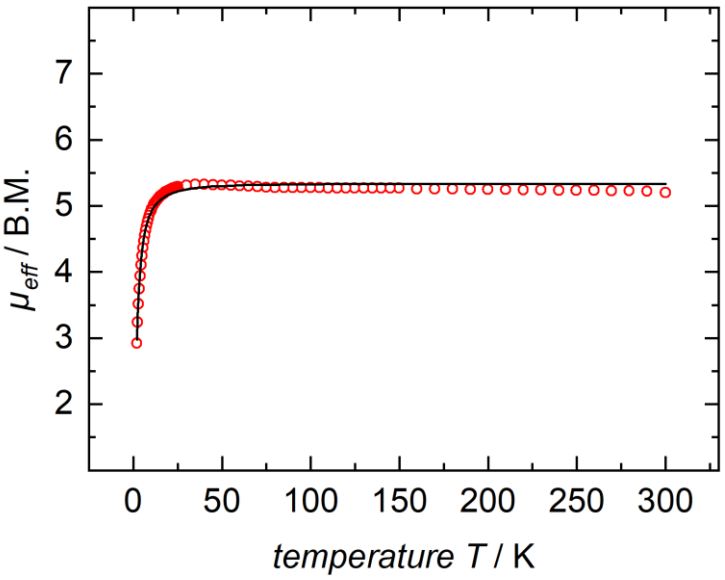

Figure S26. SQUID DC Field measurement at 1 T, 300-2 K, for ($^{t\mathrm{Bu}}$pyrpyrr$_2$)Fe(OPPh$_3$) (**1-O$^{\mathrm{Ph}}$**) sample 2 (20.2 mg, circles). The best fit (solid line) was obtained with $g_{\mathrm{av}} = 2.18$ and $|D| = 8$ cm^{-1}.

7.3 Combined SQUID Plot of (^{tBu}pyrpyrr$_2$)Fe(OPPh$_3$) (1-O^{Ph}) Sample 1 and Sample 2

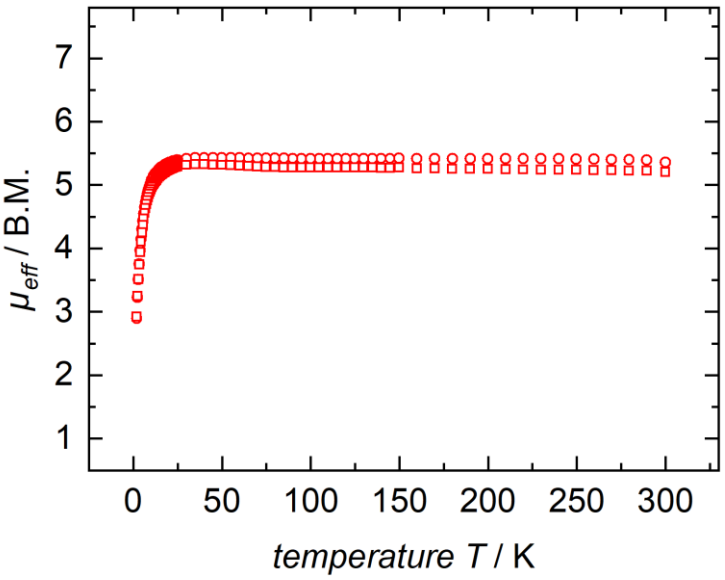

Figure S27. SQUID DC Field measurements at 1 T, 300-2 K for (^{tBu}pyrpyrr$_2$)Fe(OPPh$_3$) (**1-O^{Ph}**) sample 1 (33.9 mg, circles) and sample 2 (22.2 mg, squares).

7.4 SQUID Plot of ($^{t\text{Bu}}$pyrpyrr$_2$)Fe(SPPh$_3$) (1-S$^{\text{Ph}}$) Sample 1

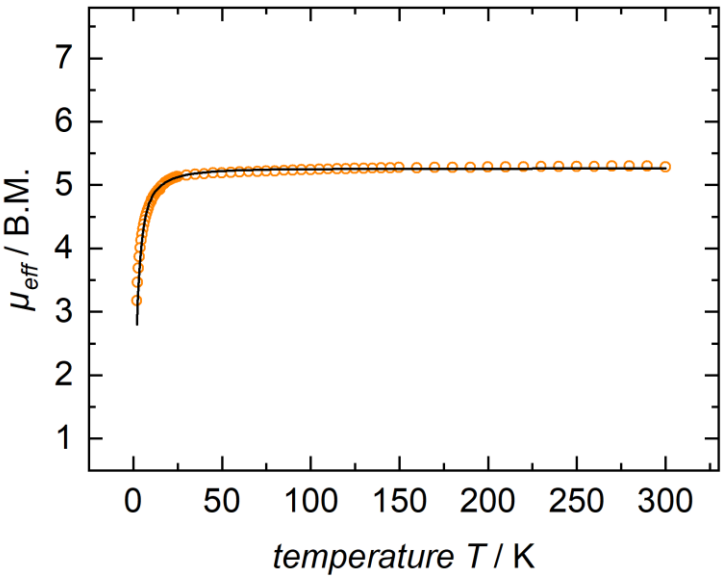

Figure S28. SQUID DC Field measurements at 1 T, 300-2 K, for ($^{t\text{Bu}}$pyrpyrr$_2$)Fe(SPPh$_3$) (**1-S$^{\text{Ph}}$**) sample 1 (4.8 mg, circles). The best fit (solid line) was obtained with $g_{\text{av}} = 2.15$, $|D| = 9$ cm^{-1}.

7.5 SQUID Plot of ($^{t\mathrm{Bu}}$pyrpyrr$_2$)Fe(SPPh$_3$) (1-S$^{\mathrm{Ph}}$) Sample 2

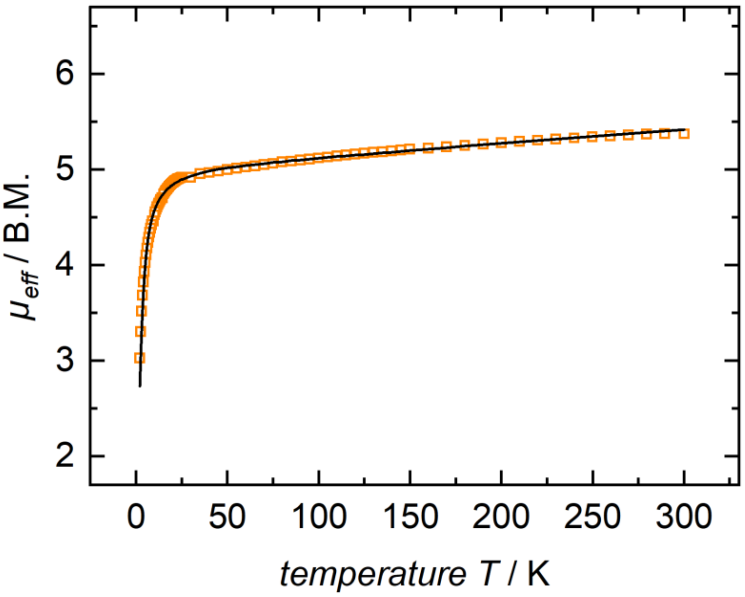

Figure S29. SQUID DC Field measurements at 1 T, 300-2 K, for ($^{t\mathrm{Bu}}$pyrpyrr$_2$)Fe(SPPh$_3$) (**1-S$^{\mathrm{Ph}}$**) sample 2 (12.3 mg, circles). The best fit (solid line) was obtained with $g_{av} = 2.03$, $|D| = 9$ cm^{-1}, and TIP = $1900 \cdot 10^{-6}$ emu.

7.6 Combined SQUID Plot of (^{tBu}pyrpyrr$_2$)Fe(SPPh$_3$) (1-S^{Ph}) Sample 1 and Sample 2

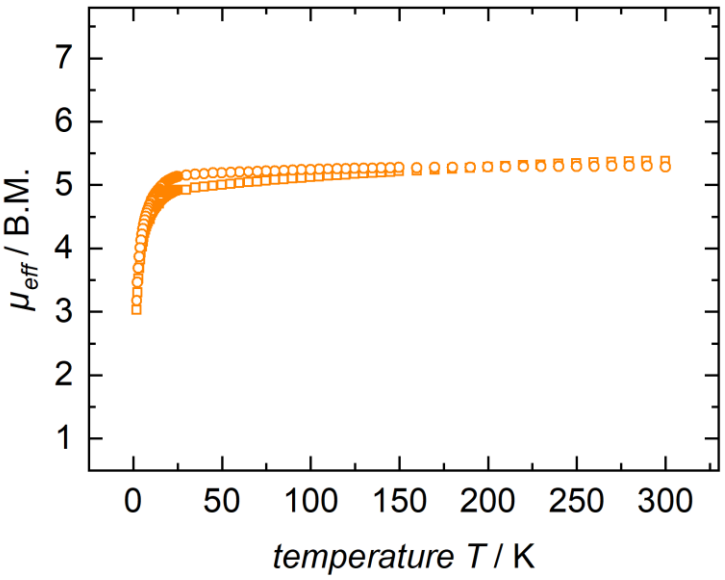

Figure S30. SQUID DC Field measurements at 1 T, 300-2 K of two representative samples of ($^{t\text{Bu}}$pyrpyrr$_2$)Fe(SPPh$_3$) (**1-S^{Ph}**). Sample 1 (4.8 mg, circles) and sample 2 (12.3 mg, squares; TIP subtracted).

7.7 SQUID Plot of ($^{t\text{Bu}}$pyrpyrr$_2$)Fe(SePPh$_3$) (1-Se$^{\text{Ph}}$) Sample 1

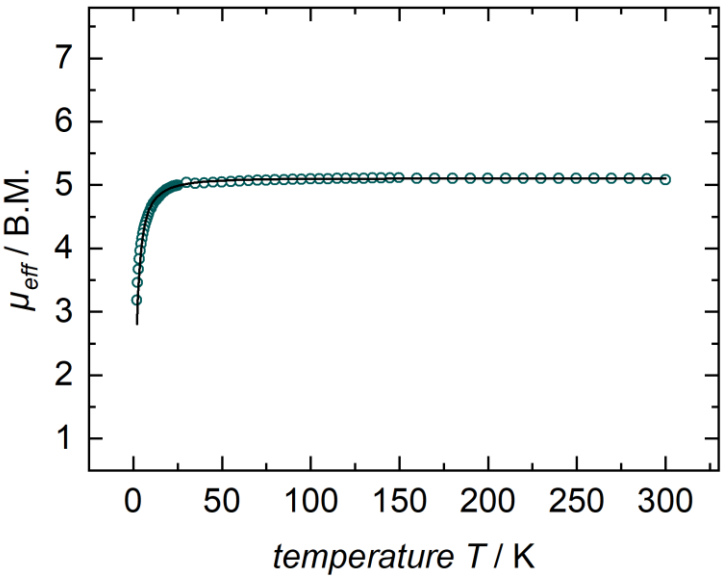

Figure S31. SQUID DC Field measurement at 1 T, 300-2 K, for ($^{t\text{Bu}}$pyrpyrr$_2$)Fe(SePPh$_3$) (**1-Se$^{\text{Ph}}$**) sample 1 (10.8 mg, circles). The best fit (solid line) was obtained with $g_{av} = 2.08$, $|D| = 9$ cm^{-1}.

7.8 SQUID Plot of ($^{t\mathrm{Bu}}$pyrpyrr$_2$)Fe(SePPh$_3$) (1-Se$^{\mathrm{Ph}}$) Sample 2

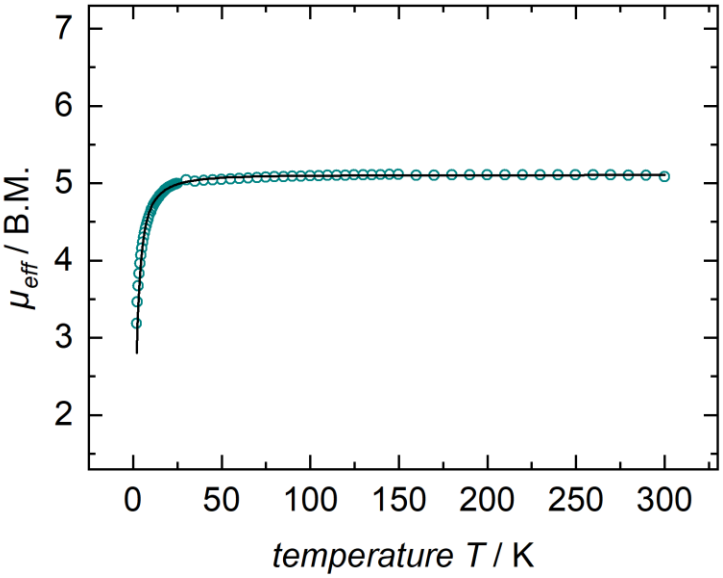

Figure S32. SQUID DC Field measurements at 1 T, 300-2 K, for ($^{t\mathrm{Bu}}$pyrpyrr$_2$)Fe(SePPh$_3$) (**1-Se$^{\mathrm{Ph}}$**) sample 2 (8.2 mg, circles). The best fit (solid line) was obtained with $g_{\mathrm{av}} = 2.07$, $|D| = 9$ cm^{-1}, and TIP = $700 \cdot 10^{-6}$ emu.

7.9 Combined SQUID Plot of (^{tBu}pyrpyrr$_2$)Fe(SePPh$_3$) (1-S^{Ph}) Sample 1 and Sample 2

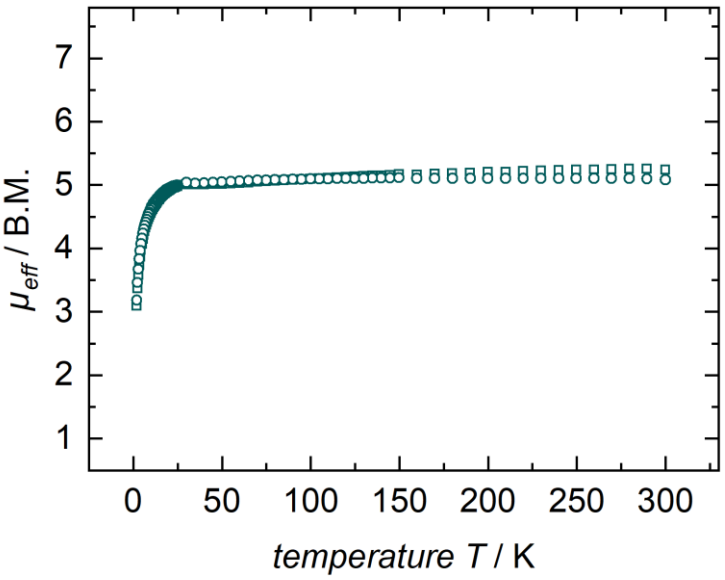

Figure S33. SQUID DC Field measurements at 1 T, 300-2 K for (^{tBu}pyrpyrr$_2$)Fe(SePPh$_3$) (**1-Se^{Ph}**) sample 1 (10.8 mg, circles) and sample 2 (8.2 mg, squares, TIP subtracted).

7.10 SQUID Plot of ($^{t\mathrm{Bu}}$pyrpyrr$_2$)Fe(TeP^{t}Bu$_3$) (1-Te$^{t\mathrm{Bu}}$) Sample 1

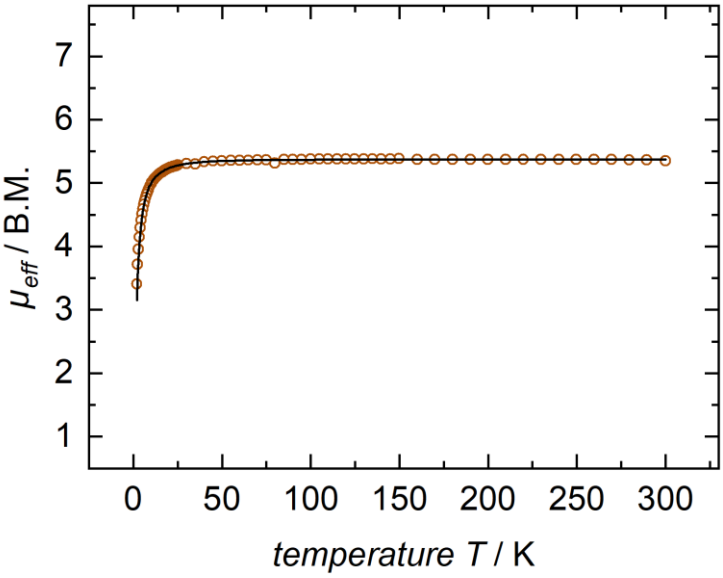

Figure S34. SQUID DC Field measurements at 1 T, 300-2 K, for ($^{t\mathrm{Bu}}$pyrpyrr$_2$)Fe(TeP^{t}Bu$_3$) (**1-Te$^{t\mathrm{Bu}}$**) sample 1 (19.2 mg, circles). The best fit obtained (solid line) was obtained with g_{av} = 2.20, $|D|$ = 8 cm^{-1}, and TIP = 3900·10^{-6} emu.

7.11 SQUID Plot of ($^{t\mathrm{Bu}}$pyrpyrr$_2$)Fe(TeP^{t}Bu$_3$) (1-Te$^{t\mathrm{Bu}}$) Sample 2

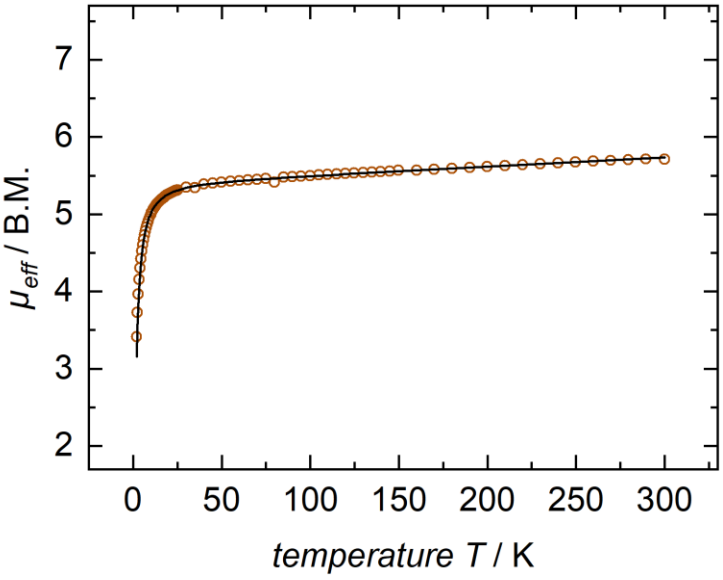

Figure S35. SQUID DC Field measurement at 1 T, 300-2 K, for ($^{t\mathrm{Bu}}$pyrpyrr$_2$)Fe(TeP^{t}Bu$_3$) (**1-Te$^{t\mathrm{Bu}}$**) sample 2 (19.7 mg, circles). The best fit obtained (solid line) was obtained with g_{av} = 2.19, $|D|$ = 8 cm^{-1}, and TIP = 1700·10^{-6} emu.

7.12 Combined SQUID Plot of (^{tBu}pyrpyrr$_2$)Fe(TeP^{t}Bu$_3$) (1-Te^{tBu}) Sample 1 and Sample 2

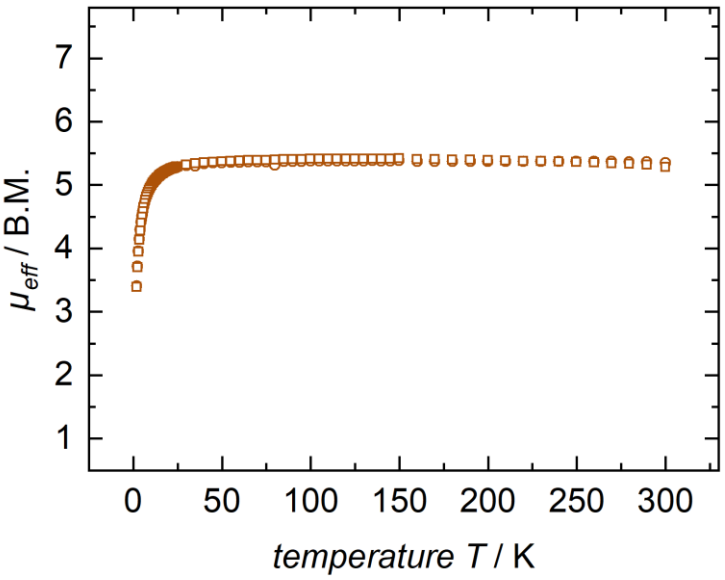

Figure S36. SQUID DC Field measurements at 1 T, 300-2 K for (^{tBu}pyrpyrr$_2$)Fe(TeP^{t}Bu$_3$) (**1-Te^{tBu}**) sample 1 (19.7 mg, circles, TIP subtracted) and sample 2 (19.2 mg, squares, TIP subtracted).

7.13 SQUID Plot of $[K]_2[(^{tBu}pyrpyrr_2)Fe_2(\mu\text{-}O)]$ (2-O) Sample 1

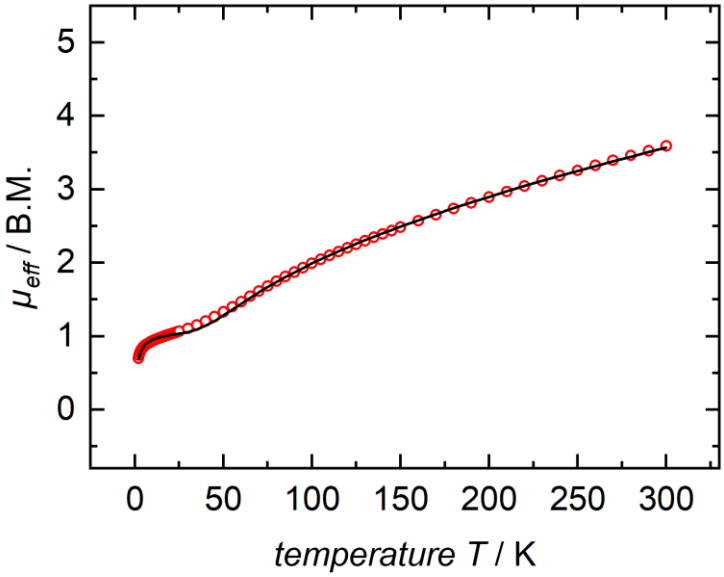

Figure S37. SQUID DC Field measurement at 1 T, 300-2 K, for $[K]_2[(^{tBu}pyrpyrr_2)Fe_2(\mu\text{-}O)]$ **(2-O)** sample 1 (24.2 mg, circles). The best fit (solid line) was obtained with g_{av} = 2.05 and J = –65 cm^{-1}. The shoulder around 10 K was simulated assuming a paramagnetic impurity (S = 2.5, Θ = –3 K) making up for 3% of the bulk material.

7.14 Combined SQUID Plot of $[K]_2[(^{tBu}pyrpyrr_2)Fe_2(\mu\text{-}O)]$ (2-O) Sample 1 and Sample 2

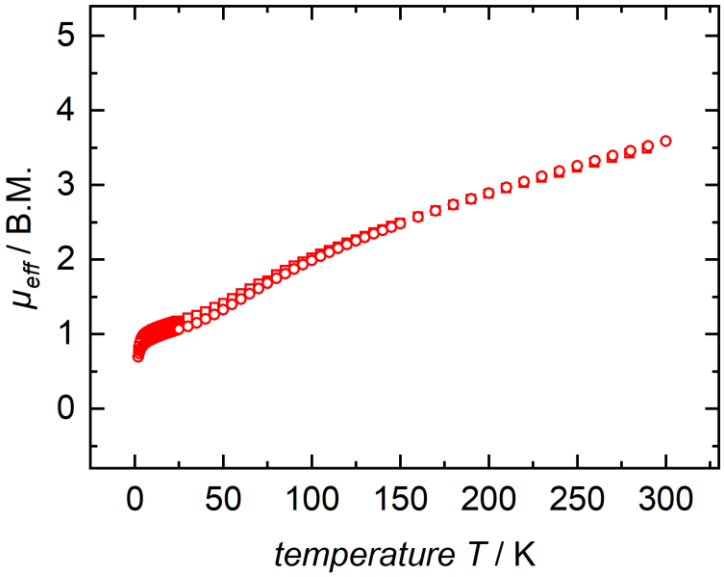

Figure S18. SQUID DC Field measurements at 1 T, 300-2 K of two representative samples of $[K]_2[(^{tBu}pyrpyrr_2)Fe_2(\mu\text{-}O)]$ **(2-O)**. Sample 1 (24.2 mg, circles) and sample 2 (24.0 mg, squares).

7.15 SQUID Plot of $[K]_2[(^{tBu}pyrpyrr_2)Fe_2(\mu\text{-}S)]$ (2-S) Sample 1

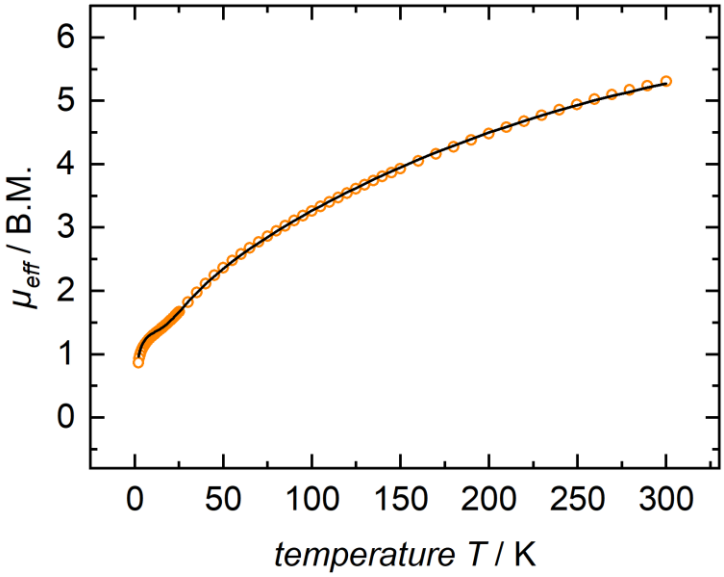

Figure S39. SQUID DC Field measurement at 1 T, 300-2 K, for $[K]_2[(^{tBu}pyrpyrr_2)Fe_2(\mu\text{-}S)]$ **(2-S)** sample 1 (22.0 mg, circles). The best fit (solid line) was obtained with g_{av} = 2.15 and J = –30 cm^{-1}[1]. The shoulder around 10 K was simulated assuming a paramagnetic impurity (S = 2.5, Θ = –3 K) making up for 7% of the bulk material.

7.16 Combined SQUID Plot of $[K]_2[(^{tBu}pyrpyrr_2)Fe_2(\mu\text{-}S)]$ (2-S) Sample 1 and Sample 2

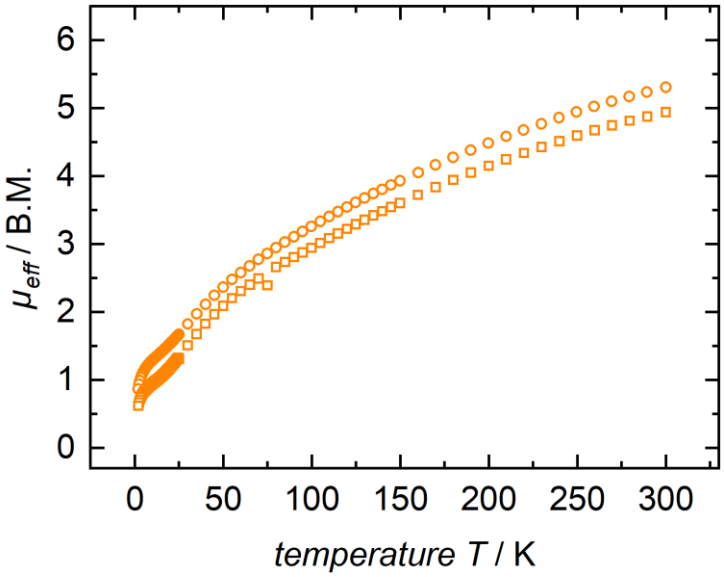

Figure S40. SQUID DC Field measurements at 1 T, 300-2 K of two representative samples of $[K]_2[(^{tBu}pyrpyrr_2)Fe_2(\mu\text{-}S)]$ **(2-S)**. Sample 1 (22.0 mg, circles) and sample 2 (18.3 mg, squares).

7.17 VTVF SQUID Plot of $[K]_2[(^{tBu}pyrpyrr_2)Fe_2(\mu\text{-}S)]$ (2-S) Sample 1

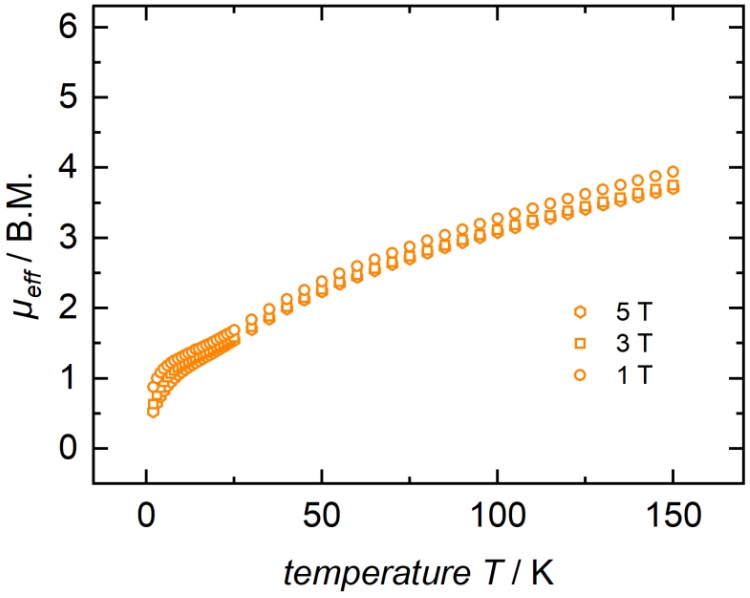

Figure S41. SQUID DC field VTVF measurement for $[K]_2[(^{tBu}pyrpyrr_2)Fe_2(\mu\text{-}S)]$ **(2-S)** sample 1 (22.0 mg), measured at 5 T, 3 T, 1 T and 0.1 T (2-150 K).

7.18 SQUID Plot of $[K]_2[(^{tBu}pyrpyrr_2)Fe_2(\mu\text{-}Se)]$ (2-Se) Sample 1

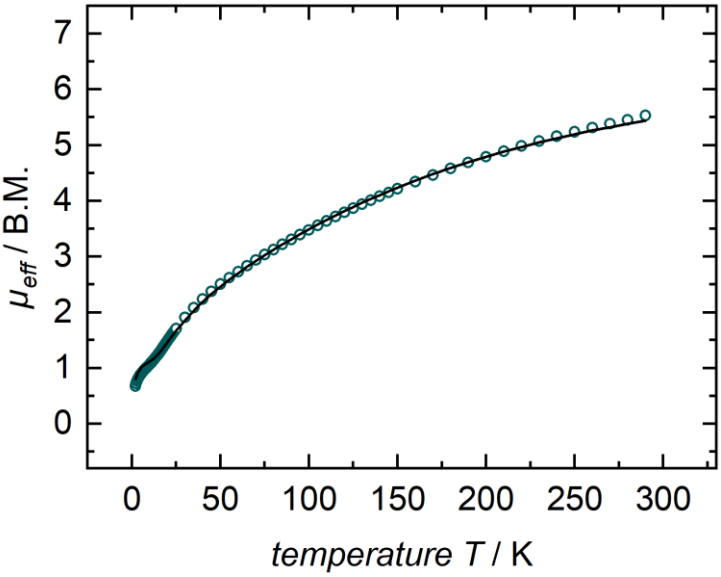

Figure S42. SQUID DC Field measurement at 1 T, 300-2 K, for $[K]_2[(^{tBu}pyrpyrr_2)Fe_2(\mu\text{-}Se)]$ **(2-Se)** sample 1 (24.4 mg, circles). The best fit (solid line) was obtained with g_{av} = 2.08 (fixed) and J = – 24 cm^{-1}. The shoulder around 10 K was simulated assuming a paramagnetic impurity (S = 2.5, Θ = –3 K) making up for 5% of the bulk material.

7.19 Combined SQUID Plot of [K]$_2$[($^{t\text{Bu}}$pyrpyrr$_2$)Fe$_2$(μ-Se)] (2-Se) Sample 1 and Sample 2

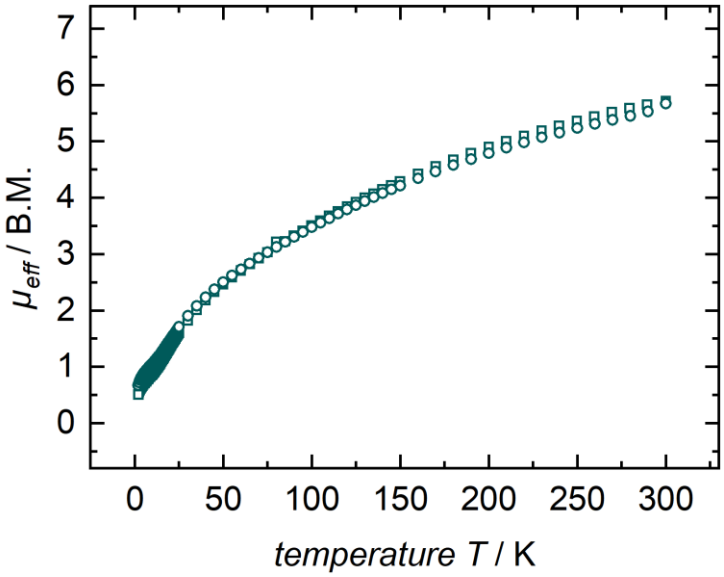

Figure S43. SQUID DC Field measurements at 1 T, 300-2 K of two representative samples of [K]$_2$[($^{t\text{Bu}}$pyrpyrr$_2$)Fe$_2$(μ-Se)] **(2-Se)**. Sample 1 (24.4 mg, circles) and sample 2 (22.7 mg, squares).

7.20 VTVF SQUID Plot of $[K]_2[(^{tBu}pyrpyrr_2)Fe_2(\mu\text{-}Se)]$ (2-Se) Sample 1

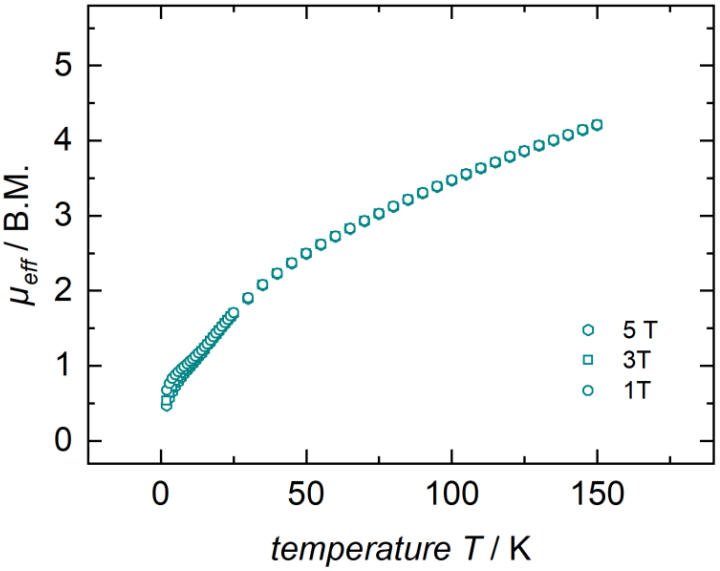

Figure S44. SQUID DC field VTVF measurement for $[K]_2[(^{tBu}pyrpyrr_2)Fe_2(\mu\text{-}Se)]$ **(2-Se)** sample 1 (24.4 mg), measured at 5 T, 3 T, and 1 T (2-150 K).

7.21 SQUID Plot of $[K]_2[(^{tBu}pyrpyrr_2)Fe_2(\mu\text{-}Te)]$ (2-Te) Sample 1

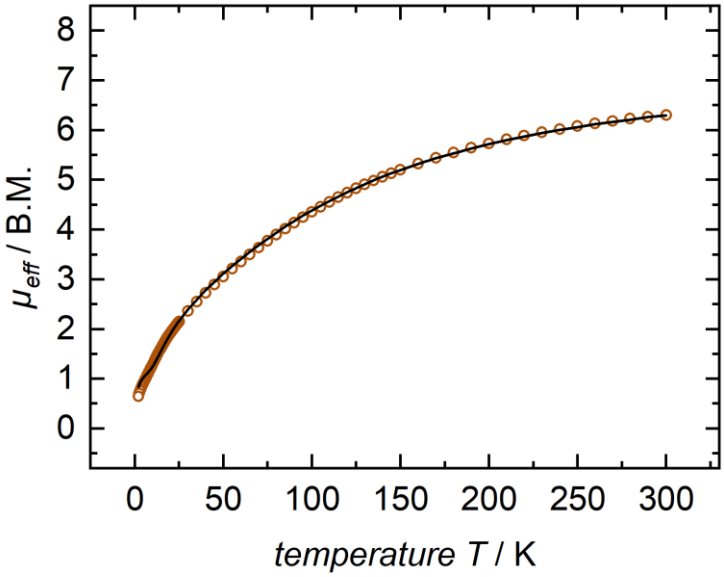

Figure S45. SQUID DC Field measurement at 1 T, 300-2 K, for $[K]_2[(^{tBu}pyrpyrr_2)Fe_2(\mu\text{-}Te)]$ **(2-Te)** sample 1 (27.6 mg, circles). The best fit was obtained with g_{av} = 2.19 (fixed) and J = –16 cm^{-1}. The shoulder around 10 K was simulated assuming a paramagnetic impurity (S = 2.5, Θ = –3 K) making up for 5% of the bulk material.

7.22 Combined SQUID Plot of $[K]_2[(^{tBu}pyrpyrr_2)Fe_2(\mu\text{-}Te)]$ (2-Te) Sample 1 and Sample 2

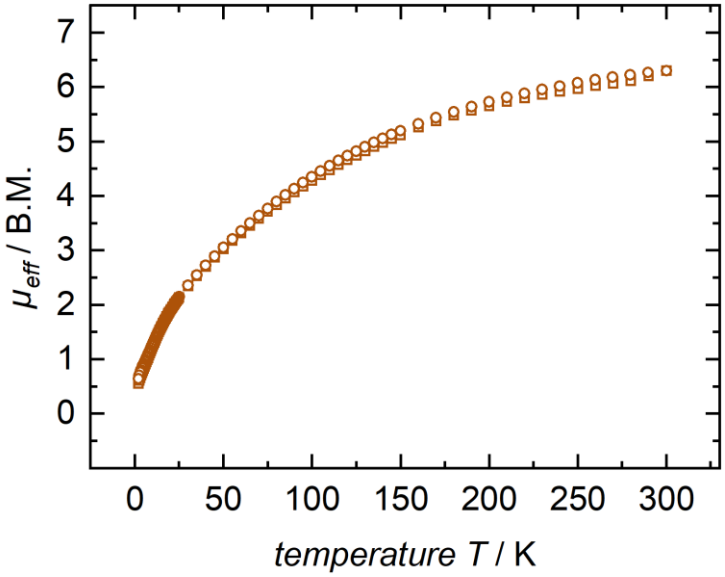

Figure S46. SQUID DC Field measurements at 1 T, 300-2 K of two representative samples of $[K]_2[(^{tBu}pyrpyrr_2)Fe_2(\mu\text{-}Te)]$ **(2-Te)**. Sample 1 (27.6 mg, circles) and sample 2 (26.5 mg, squares).

8 Crystallographic Information

Table S1. X-Ray crystallographic data for **1-O^{Ph}**·pentane, **1-S^{Ph}**·toluene, **1-Se^{Ph}**·CH_2Cl_2, and **1-Te^{tBu}**.

	1-O^{Ph}·pentane	**1-S^{Ph}**·toluene	**1-Se^{Ph}**·CH_2Cl_2	**1-Te^{tBu}**
Empirical formula	$C_{52}H_{68}FeN_3OP$	$C_{54}H_{64}FeN_3PS$	$C_{48}H_{58}Cl_2FeN_3PSe$	$C_{41}H_{68}FeN_3PTe$
Formula weight	837.91	873.96	913.65	817.40
Temperature/K	100	100	100	100
Crystal system	monoclinic	monoclinic	triclinic	monoclinic
Space group	$P2_1/n$	$P2_1/n$	$P\bar{1}$	$P2_1/n$
Cell Constants				
a	15.9812(2)Å	9.82150(10)Å	9.80500(10)Å	10.26880(10)Å
b	16.29860(10)Å	24.9832(3)Å	14.5687(2)Å	24.3657(2)Å
c	18.9525(2)Å	19.1363(3)Å	17.0188(2)Å	16.74400(10)Å
β	111.3550(10)°	101.2200(10)°	91.1460(10)°	97.6970(10)°
Volume	4597.64(9)Å^3	4605.78(10)Å^3	2213.03(5)Å^3	4151.71(6)Å^3
Z	4	4	2	4
d_{calc}	1.211 g/cm^3	1.260 g/cm^3	1.371 g/cm^3	1.308 g/cm^3
μ	3.256 mm^{-1}	0.447 mm^{-1}	1.357 mm^{-1}	1.121 mm^{-1}
F(000)	1800.0	1864.0	952.0	1712.0
Crystal size, mm	0.33 × 0.12 × 0.04	0.49 × 0.21 × 0.06	0.54 × 0.3 × 0.1	0.25 × 0.23 × 0.14
2θ range for data collection	6.22 - 148.982°	3.916 - 54.968°	4.422 - 54.968°	4.148 - 54.97°
Index ranges	$-19 \le h \le 19$, $-20 \le k \le 20$, $-23 \le l \le 22$	$-12 \le h \le 12$, $-32 \le k \le 32$, $-24 \le l \le 24$	$-12 \le h \le 12$, $-18 \le k \le 18$, $-21 \le l \le 22$	$-13 \le h \le 13$, $-31 \le k \le 31$, $-21 \le l \le 21$
Reflections collected	73300	145777	84205	148639
Independent reflections	9320[R(int) = 0.0514]	10564[R(int) = 0.0574]	10089[R(int) = 0.0572]	9519[R(int) = 0.0694]
Absorption Correction	Semi-empirical from equivalents	Semi-empirical from equivalents	Semi-empirical from equivalents	Semi-empirical from equivalents
Refinement Method	Full-matrix least-squares on F^2	Full-matrix least-squares on F^2	Full-matrix least-squares on F^2	Full-matrix least-squares on F^2
Data/restraints/parameters	9320/0/537	10564/204/575	10089/0/547	9519/0/445
Goodness-of-fit on F^2	1.085	1.028	1.069	1.049
Final R indexes [I>=2σ (I)]	R_1 = 0.0352, wR_2 = 0.0927	R_1 = 0.0553, wR_2 = 0.1529	R_1 = 0.0361, wR_2 = 0.0802	R_1 = 0.0495, wR_2 = 0.1317
Final R indexes [all data]	R_1 = 0.0392, wR_2 = 0.0953	R_1 = 0.0656, wR_2 = 0.1590	R_1 = 0.0472, wR_2 = 0.0836	R_1 = 0.0539, wR_2 = 0.1351
Largest diff. peak/hole	0.30/-0.55 eÅ^{-3}	1.64/-1.27 eÅ^{-3}	0.82/-0.63 eÅ^{-3}	2.91/-2.14 eÅ^{-3}

Table S2. X-Ray crystallographic data for **2-O**·3 toluene, **2-S**·2 Et_2O, **2-Se** 2 Et_2O, and **2-Te**·Et_2O, toluene.

	2-O·3 toluene	**2-S**·2 Et_2O	**2-Se**·2 Et_2O	**2-Te**·Et_2O, toluene
Empirical formula	$C_{79}H_{106}Fe_2K_2N_6O$	$C_{66}H_{102}Fe_2K_2N_6O_2S$	$C_{66}H_{102}Fe_2K_2N_6O_2Se$	$C_{69}H_{100}Fe_2K_2N_6OTe$
Formula weight	1345.59	1233.49	1280.39	1347.04
Temperature/K	100	100	100	100
Crystal system	monoclinic	triclinic	triclinic	monoclinic
Space group	C2/c	$P\bar{1}$	$P\bar{1}$	$P2_1$
Cell Constants				
a	23.3804(2)Å	14.11360(10)Å	14.13070(10)Å	10.5924(2)Å
b	13.85310(10)Å	15.18690(10)Å	15.18640(10)Å	20.9429(3)Å
c	23.00070(10)Å	16.72980(10)Å	16.75930(10)Å	15.9207(3)Å
β	98.8250(10)°	102.8060(10)°	102.7920(10)°	104.292(2)°
Volume	7361.53(9)Å^3	3361.61(4)Å^3	3375.48(4)Å^3	3422.47(11)Å^3
Z	4	2	2	2
d_{calc}	1.214 g/cm^3	1.219 g/cm^3	1.260 g/cm^3	1.307 g/cm^3
μ	0.554 mm^{-1}	0.632 mm^{-1}	1.137 mm^{-1}	1.008 mm^{-1}
F(000)	2880.0	1324.0	1360.0	1412.0
Crystal size, mm	0.327 × 0.283 × 0.218	0.37 × 0.27 × 0.17	0.3 × 0.15 × 0.1	0.16 × 0.1 × 0.08
2θ range for data collection	3.74 - 54.966°	3.866 - 54.968°	3.854 - 54.968°	4.42 - 56.562°
Index ranges	$-30 \le h \le 30$, $-17 \le k \le 17$, $-29 \le l \le 29$	$-18 \le h \le 18$, $-19 \le k \le 19$, $-21 \le l \le 21$	$-18 \le h \le 18$, $-19 \le k \le 19$, $-21 \le l \le 21$	$-14 \le h \le 14$, $-27 \le k \le 27$, $-21 \le l \le 21$
Reflections collected	131883	123022	128234	104462
Independent reflections	8435[R(int) = 0.0376]	15347[R(int) = 0.0450]	15398[R(int) = 0.0502]	16953[R(int) = 0.0566]
Absorption Correction	Semi-empirical from equivalents	Semi-empirical from equivalents	Semi-empirical from equivalents	Semi-empirical from equivalents
Refinement Method	Full-matrix least-squares on F^2	Full-matrix least-squares on F^2	Full-matrix least-squares on F^2	Full-matrix least-squares on F^2
Data/restraints/parameters	8435/0/422	15347/0/740	15398/90/764	16953/1/757
Goodness-of-fit on F^2	1.029	1.054	1.039	1.056
Final R indexes [I>=2σ (I)]	R_1 = 0.0470, wR_2 = 0.1357	R_1 = 0.0318, wR_2 = 0.0772	R_1 = 0.0314, wR_2 = 0.0714	R_1 = 0.0253, wR_2 = 0.0583
Final R indexes [all data]	R_1 = 0.0508, wR_2 = 0.1386	R_1 = 0.0372, wR_2 = 0.0798	R_1 = 0.0406, wR_2 = 0.0743	R_1 = 0.0277, wR_2 = 0.0621
Largest diff. peak/hole	2.00/-0.66 eÅ^{-3}	0.42/-0.32 eÅ^{-3}	0.51/-0.36 eÅ^{-3}	0.69/-0.31 eÅ^{-3}

9 References

(1) Komine, N.; Buell, R. W.; Chen, C.-H.; Hui, A. K.; Pink, M.; Caulton, K. G. Probing the Steric and Electronic Characteristics of a New Bis-Pyrrolide Pincer Ligand. *Inorg. Chem.* **2014**, *53* (3), 1361–1369.

(2) Broere, D. L. J.; Čorić, I.; Brosnahan, A.; Holland, P. L. Quantitation of the THF Content in Fe[N(SiMe3)2]2·xTHF. *Inorg. Chem.* **2017**, *56* (6), 3140–3143.

(3) Sorsche, D.; Miehlich, M. E.; Searles, K.; Gouget, G.; Zolnhofer, E. M.; Fortier, S.; Chen, C.-H.; Gau, M.; Carroll, P. J.; Murray, C. B.; et al. Unusual Dinitrogen Binding and Electron Storage in Dinuclear Iron Complexes. *J. Am. Chem. Soc.* **2020**, *142* (18), 8147–8159.

(4) Searles, K.; Fortier, S.; Khusniyarov, M. M.; Carroll, P. J.; Sutter, J.; Meyer, K.; Mindiola, D. J.; Caulton, K. G. A Cis-Divacant Octahedral and Mononuclear Iron(IV) Imide. *Angew. Chemie Int. Ed.* **2014**, *53* (51), 14139–14143.

(5) Altintas, O.; Glassner, M.; Rodriguez-Emmenegger, C.; Welle, A.; Trouillet, V.; Barner-Kowollik, C. Macromolecular Surface Design: Photopatterning of Functional Stable Nitrile Oxides. *Angew. Chemie Int. Ed.* **2015**, *54* (19), 5777–5783.

(6) Bartlett, P. D.; Meguerian, G. Reactions of Elemental Sulfur. I. The Uncatalyzed Reaction of Sulfur with Triarylphosphines1. *J. Am. Chem. Soc.* **1956**, *78* (15), 3710–3715.

(7) Malito, J.; Alyea, E. C. STERIC AND ELECTRONIC DESTABILIZATION OF THE P—Se BOND IN TRIARYLPHOSPHINE SELENIDE SYSTEMS. *Phosphorus. Sulfur. Silicon Relat. Elem.* **1990**, *54* (1–4), 95–99.

(8) Kuhn, N.; Schumann, H.; Wolmershäuser, G. (Tert-C4H9)3 PTe — Ein Typisches Tellurophosphoran? [1] / (Ferr-C4H9)3 PTe -a Typical Tellurophosphorane? [1]. *Zeitschrift für Naturforsch. B* **1987**, *42* (6), 674–678.

(9) Schubert, E. M. Utilizing the Evans Method with a Superconducting NMR Spectrometer in the Undergraduate Laboratory. *J. Chem. Educ.* **1992**, *69* (1), 62.

(10) Bill, E. Mössbauer Program Mcal. 2019.

(11) Bain, G. A.; Berry, J. F. Diamagnetic Corrections and Pascal's Constants. *J. Chem. Educ.* **2008**, *85* (4), 532.

(12) Bill, E. SQUID Program JulX2. 2019.